where

a =area of cross-section, in

r = radius of gyration, in

t_4 = gusset-plate thickness, in

ℓ = width of gusset, in

and

$$f = \frac{P}{a} = \frac{18000}{1 + (h^2/18000r^2)} \quad \text{if } 60 < h/r < 200 \tag{5.68}$$

where

h = height of gusset, in

From Equations (5.66), (5.67) and (5.68) we may obtain

$$18{,}000\,\ell t_4^3 - (\text{bolt load})\,t_4^2 - \frac{h^2(\text{bolt load})}{1{,}500} = 0 \tag{5.69}$$

If h is small the third term in the equation may be disregarded, therefore simplifying Equation (5.69) to

$$t_4 = \frac{\text{bolt load}}{18{,}000\,\ell} \tag{5.70}$$

When an external bolting chair is used the thickness of the stack shell, t, at the base should be checked. To determine the thickness Equation (5.71) can be used

$$t = 1.76\left(\frac{P_a}{mh\,f_{all}}\right)^{2/3} r^{1/3} \tag{5.71}$$

where

r = radius of the stack at the point under consideration, inches

P = maximum bolt load, pounds

a = radial distance from outside of stack shell to the anchor bolt circle, inches

h = gusset height, inches

m = 2A (see Figure 5.14) or bolt spacing

5.6 Approximate Breech Opening Analysis

From a functional point of view, steel stacks have to resist the effects of wind and of their own weight. In the case of steel stacks the effects of the wind predominate by a comparison of the influence of their own weight.

With respect to their structural behavior there are two types of steel stacks: the self-supporting type and guyed stacks.

The self-supporting type acts as a column resisting its own weight, acting vertically, and the overturning effect of the wind, the base only being fixed. In other words, it is a cantilever subjected to a relatively large overturning moment and a relatively small vertical load.

Guyed stacks resist the same forces, but it is assisted by lateral supports in the form of guyed cables equally spaced around the stack and anchored at the other end to concrete blocks, some distance from the stack footings. The effect of those guy cables is to produce a somewhat smaller wind bending moment in the stack.

Near the base of the stack a relatively wide *breech opening* or *flue inlet* is cut. To facilitate the inspection and lining of stacks and to enable soot, etc., to be removed, it is usual to fit an *access door* near the base. As in the case of the breech opening, any opening of this nature should be adequately reinforced.

The breech opening weakens the wall of the stack considerably and some forms of compensation are required to take the loading and provide safety against local buckling.

In the following discussion the breech opening analysis and reinforcement design are considered for self-supporting stacks. However, it should be noted that such an analysis and design may be applied to guyed stacks. This is because guyed stacks are affected by such similar loadings as self-supporting stacks. Only the vertical load may be increased on account of the vertical reactions of guy cables.

In the following are given two methods for the analysis and design of breech openings: one approximate and another more rigorous method.

An approximate method may be useful for the preliminary analysis and design and a more rigorous method is recommended for the final design [5.55].

5.6.1 Conception of the Method

Experiments show that the applied load causing the general collapse of the thin-walled cylindrical shell axially-loaded is slightly greater than load initiating local buckling. Prior to local buckling, a shell is quite sensitive to slight disturbances. When the applied load is just below the local buckling load any lateral disturbance would cause local buckling to occur in the hole region cut in the shell.

Once the local buckling had occurred, the shell did not seem as sensitive to slight disturbances because these disturbances seldom led to its general collapse. Buckling loads continued to decrease as the hole dimensions increased.

During the experimental tests the loads were applied differently by the testing machines used in shell tests and

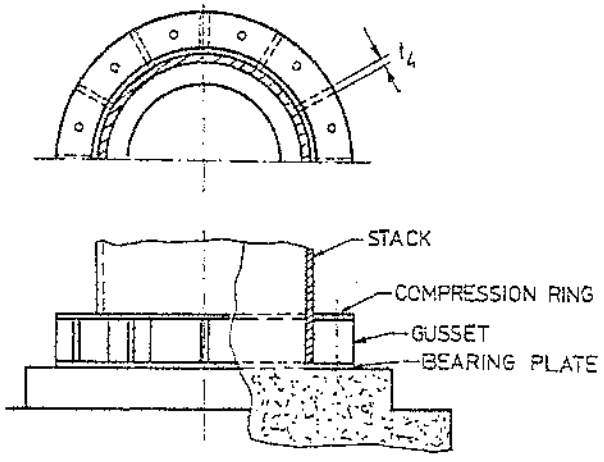

FIGURE 5.15 — Stack shell with external bolting chairs.

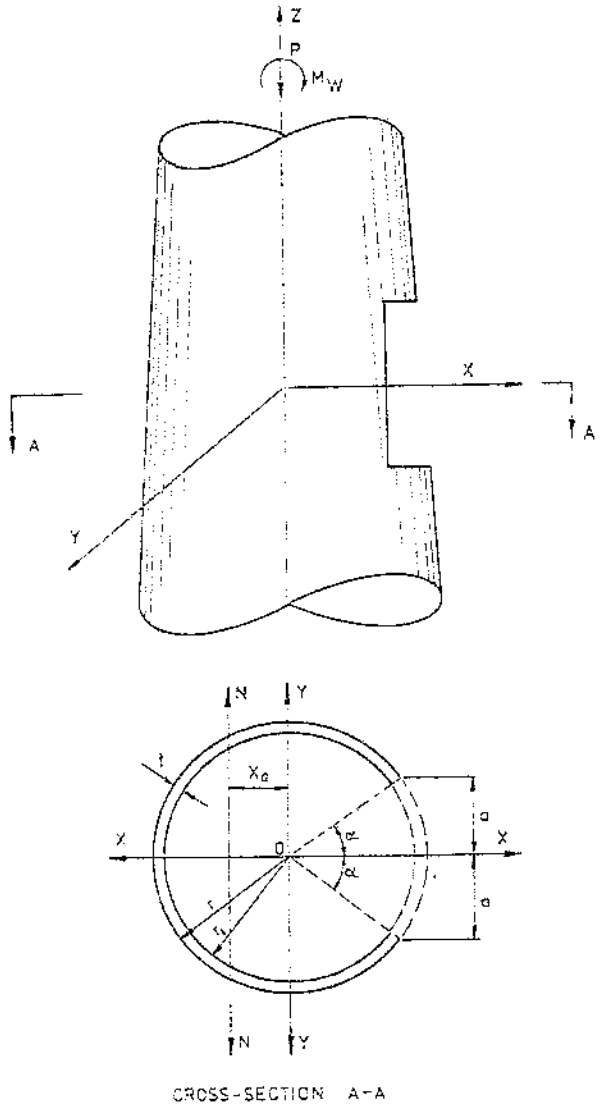

FIGURE 5.16 — Shell and hole geometry.

the measured shell buckling loads were reduced to approximate equivalent applied stresses in order to provide a common basis for comparison. This was done by replacing the applied load with a *statically-equivalent membrane stress system acting on the plane* which may be called *the applied stress plane* and which is perpendicular to the cylinder axis, Figure 5.16.

Therefore, the statically-equivalent applied membrane stress system must equilibrate the applied axial load plus a static bending moment due to wind action and eccentricity of axial load with respect to the neutral axis of cross-section.

To simplify the form of this applied membrane stress system the following assumptions were made:

a. The membrane stress applied at y = ± a, Figure 5.16, on the hole edge can be used to represent the applied stress corresponding to local buckling of the shell, and

b. The hole is far enough from the ends of the shell, so that the assumed applied stresses are not influenced by the end support conditions.

5.6.2 Stresses at the Edge of Breech Opening

Reduced cross-section of the stack shell is under influence of axial load P and wind bending moment M_W.

Based on the geometry of the applied stress plane shown in Figure 5.16, the resulting stresses in the wall of the stack are given by

$$f = -\frac{P}{A} \pm \frac{(M_W + Px_c)x}{I} \qquad (5.72)$$

where

A = reduced cross-sectional area of the stack.

I = moment of inertia of the reduced cross-sectional area of the stack

If the resulting stresses remain negative (compression only), then there will be no anomaly, and the usual laws of

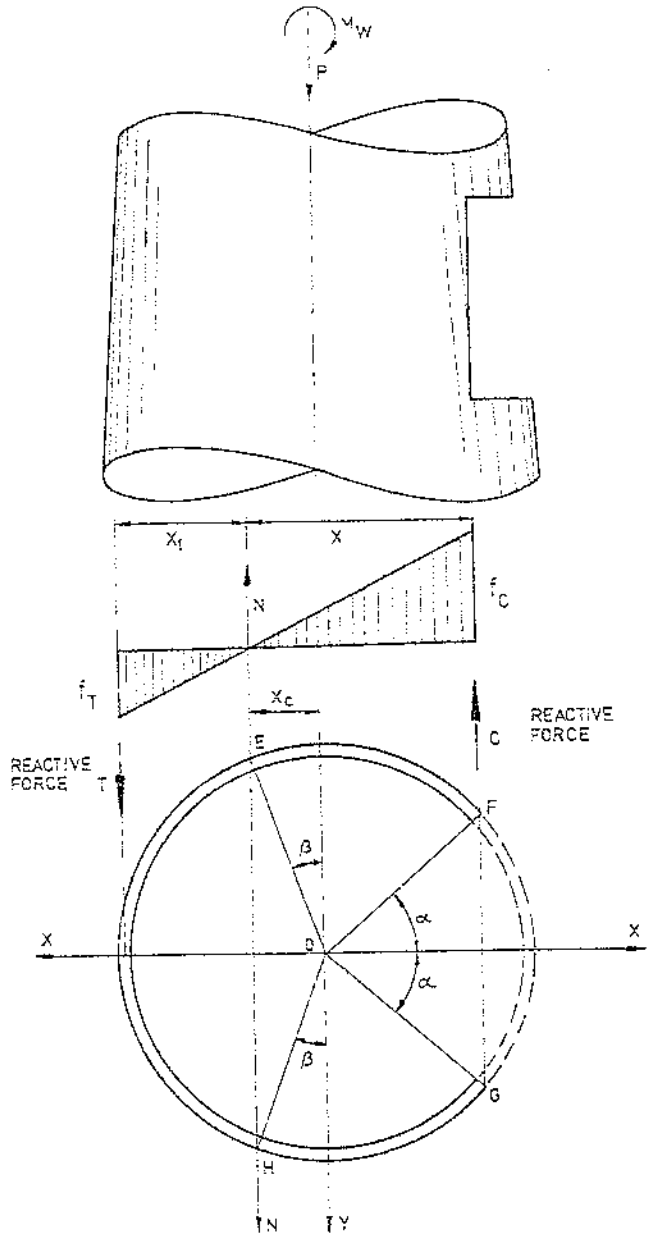

FIGURE 5.17 — Cross-section of the stack. Stress distribution diagram.

statics will be valid. If, however, the stress distribution diagram includes a tensile portion, this should be considered in further analysis, assuming that the position of neutral axis is known.

With reference to Figure 5.17, the following notations are introduced.

Sc,ST = statical moments of wall under compression and tension, respectively, referred to the neutral axis.

Ic,IT = moments of inertia of wall under compression and tension, respectively, referred to the neutral axis.

C, T = total compressive and tensile forces, respectively.

Mc,MT = moments capable of being resisted by the compressive and tensile sides, respectively.

ϕ = fT = the slope of the stress line and

$$f_c = x \frac{f_T}{x_1} \tag{5.73}$$

Then, the compressive force is

$$C = \int f_c dA = \left(\frac{f_T}{x_1}\right) \int x\, da = \phi S_c \tag{5.74}$$

By analogy, the value of tensile force is

$$T = \phi S_T \tag{5.75}$$

Bending moment capable of being resisted by the compressive area is

$$M_c = \int x f_c dA = \left(\frac{f_T}{x_1}\right) \int x^2 dA = \phi I_c \tag{5.76}$$

By analogy, the value of the bending moment capable of being resisted by the tensile are is

$$M_T = \phi I_T \tag{5.77}$$

From the condition of the equilibrium of vertical forces, we have

$$\begin{aligned} P + T - C &= 0 \\ \text{or} \qquad P &= C - T = N \end{aligned} \tag{5.78}$$

Total bending moment is

$$M = M_c + M_T = M_w + Px_o \tag{5.79}$$

After substituting into formula (5.78) values (5.74) and (5.75), we obtain

$$N = C - T = \phi\,(S_c - S_T) \tag{5.80}$$

and formula (5.79), using (5.76) and (5.77) may be represented as

$$M = M_w + Px_o = \phi\,(I_c + I_T) \tag{5.81}$$

From (5.81), the value of ϕ is

$$\phi = \frac{M_w + Px_o}{I_c + I_T} \tag{5.82}$$

The value of N determined from the formula (5.80) should be equal to P, or

$$N = \phi\,(S_c - S_T) = P \tag{5.83}$$

The average compressive stress in the wall may be obtained from the formula

$$f_{av} = \frac{C}{Lt} = \frac{\phi S_c}{Lt} \tag{5.84}$$

where L is the total length of the compressed wall, Figure 5.17

$$L = \text{arc EF} + \text{arc GH}$$

or

$$L = 2 \times \frac{\pi R(90 - \alpha + \beta)}{180} \tag{5.85}$$

Using midwall radius

$$R = \frac{r + r_1}{2} \tag{5.86}$$

we obtain

$$L = \frac{\pi(r + r_1)(90 - \alpha + \beta)}{180} \tag{5.87}$$

Therefore, the average compressive stress is

$$f_{av} = \frac{\phi S_c}{t} \frac{180}{\pi(r + r_1)(90 - \alpha + \beta)} \tag{5.88}$$

The maximum value of the compressive stress occurring at the edge of the opening can be approximately determined by considering 1 inch wide strip at the edge, Figure 2.18.

From the diagram of stresses we may find the following ratios

$$\begin{aligned} \frac{f_1}{x_1} &= \frac{f_3}{x} \quad ; \quad f_1 = x_1 \frac{f_3}{x} = \phi x_1 \\ \frac{f_2}{x_2} &= \frac{f_3}{x} \quad ; \quad f_2 = x_2 \frac{f_3}{x} = \phi x_2 \end{aligned} \tag{5.89}$$

The maximum stress at the middle of the wall is

$$f_{max} = \frac{f_1 + f_2}{2} = \frac{\phi}{2} \quad (x_1 + x_2) \tag{5.90}$$

By substituting

$$x_1 = x_6 + r\cos\alpha \; ; \; x_2 = x_6 + r_1 \cos\alpha \tag{5.91}$$

$$f_{max} = \frac{\phi}{2}\left[2x_c + (r + r_1)\cos\alpha\right]$$

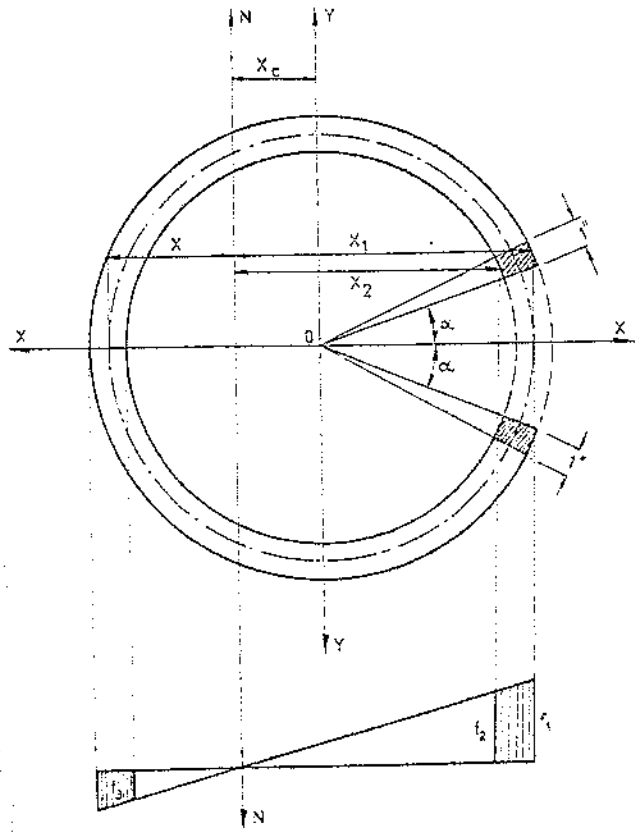

FIGURE 5.18 — Diagram of stresses in the wall of stack.

5.6.3 Geometrical Properties of the Reduced Cross-Section of the Stack

5.6.3.1 Statical Moment of the Compressed Area Figure 5.19

Ordinate of centroid of the sector AOB is

$$y_c = Y_1 + Y_2 = \frac{2r \sin\gamma_1 \sin\gamma_2}{3\gamma_1} + r \sin\beta \tag{5.92}$$

Area of the sector AOB

$$A = r^2\gamma_1 \tag{5.93}$$

Statical moment of the sector AOB is

$$S_1 = Ay_c = r^2\gamma_1 \left(\frac{2r \sin\gamma_1 \sin\gamma_2}{3\gamma_1} + r \sin\beta\right) \tag{5.94}$$

and for sector A_1OB_1

$$S_2 = r_1^2\gamma_1 \left(\frac{2r_1 \sin\gamma_1 \sin\gamma_2}{3\gamma_1} + r \sin\beta\right) \tag{5.95}$$

Total statical moment is

$$S_c = 2(S_1 - S_2) = \frac{4}{3}(r^3 - r_1^3) \sin\gamma_1 \sin\gamma_2 + 2r(r^2 - r_1^2)\gamma_1 \sin\beta \tag{5.96}$$

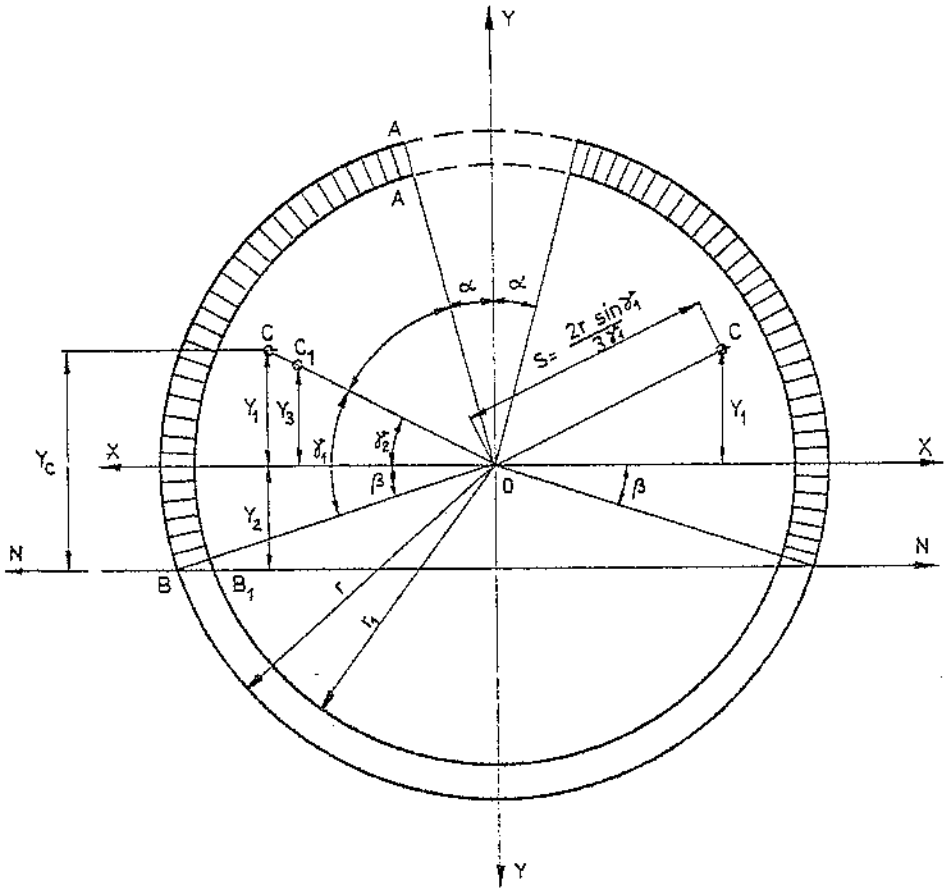

FIGURE 5.19 — Geometric data for the determination of statical moment of compressed area.

where

$$\gamma_1 = \frac{90 - \alpha + \beta}{2} \qquad (5.97)$$

$$\gamma_2 = \frac{90 - \alpha - \beta}{2} \qquad (5.98)$$

5.6.3.2 Statical Moment of Tensile Area: Figure 5.20

Ordinate of centroid of segment DEF

$$y_c = \frac{4\ r\ \cos^3\beta}{3\ [2(90-\beta) - \sin 2\beta]} \qquad (5.99)$$

Area of the segment DEF is

$$A = \frac{r^2}{2}\left[2(90 - \beta) - \sin 2\beta\right] \qquad (5.100)$$

Statical moment of the segment DEF with respect to the neutral axis N-N is

$$S_1 = A\ (y_c - r \sin\beta) =$$

$$= \frac{r^2}{2}\left[2\ (90-\beta) - \sin 2\beta\right] \times$$

$$\times \left\{\frac{4r\ \cos^3\beta}{3\ [2(90-\beta) - \sin 2\beta)]} - r \sin\beta\right\} =$$

$$S_1 = \frac{r^2}{2}\left\{\frac{4}{3}\ r\ \cos^3\beta - r \sin\beta\left[2(90-\beta) - \sin 2\beta\right]\right\} \qquad (5.101)$$

By analogy, statical moment of the segment $D_1E_1F_1$ with respect to the neutral axis N-N is

$$S_2 = \frac{r_1^2}{2}\left\{\frac{4}{3}\ r_1\ \cos^3\beta - r \sin\beta\left[2(90-\beta) - \sin 2\beta\right]\right\} \qquad (5.102)$$

Total statical moment of the tensile area with respect to neutral axis N-N is

$$S_T = S_1 - S_2 = \frac{2}{3}\ (r^3 - r_1^3)\ \cos^3\beta -$$

$$- \frac{r}{2}\ (r^2 - r_1^2)\ \sin\beta \times \left[2(90-\beta) - \sin 2\beta\right] \qquad (5.103)$$

5.6.3.3 Moment of Inertia of the Compressed Area; Figure 5.21

The moment of inertia of the compressed area with respect to the neutral axis N-N is

$$I_N = I_x + A\ (y_c^2 - y_1^2) \qquad (5.104)$$

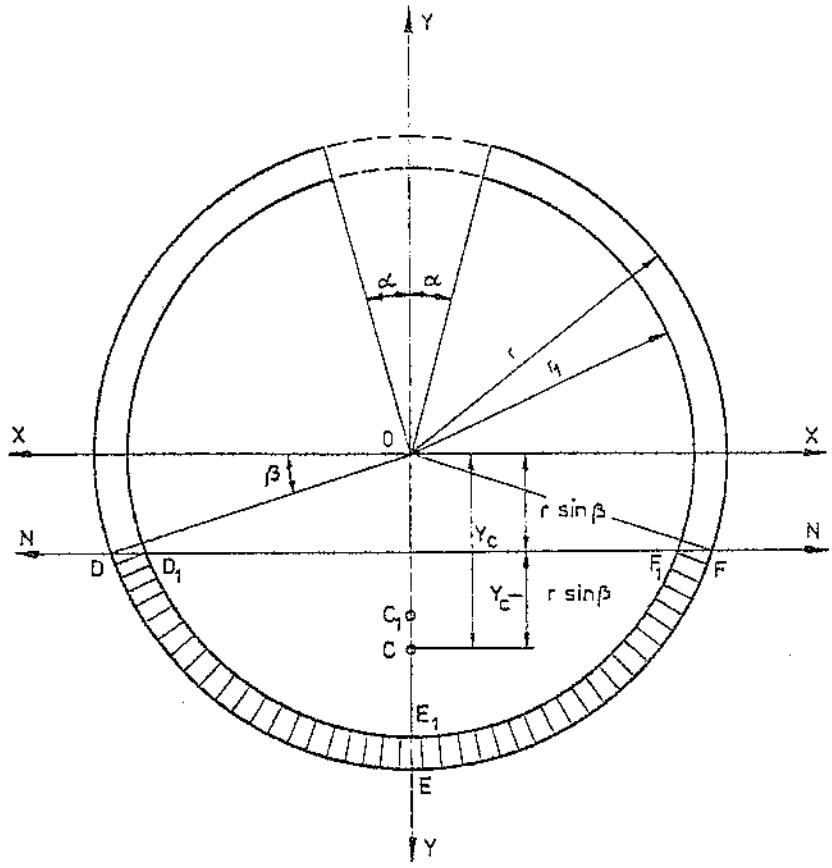

FIGURE 5.20 — Geometric data for determination of statical moment of tensile area.

a. *Moments of inertia of two sections AOB with respect to neutral axis x-x are*

$$I_{1x} = 2\int_{0}^{r}\int_{\alpha}^{90+\beta}(Rd\phi dR)(R\cos\phi)^2 =$$

$$= 2\int_{0}^{r}R^3dR\int_{\alpha}^{90+\beta}\cos^2\phi d\phi = \qquad (5.105)$$

$$= \frac{r^4}{4}\left[2\gamma_1 - \sin(\alpha+\beta)\cos(\alpha-\beta)\right]$$

where $$\gamma_1 = \frac{90 - \alpha + \beta}{2} \qquad (5.106)$$

By analogy, the moments of inertia of two sectors A_1OB_1 with respect to neutral axis x-x are

$$I_{2x} = \frac{r_1^4}{4}\left[2\gamma_1 - \sin(\alpha+\beta)\cos(\alpha-\beta)\right] \qquad (5.107)$$

Therefore, the moments of inertia of two rings AA_1BB_1 are

$$I_x = I_{1x} - I_{2x} =$$

$$= \frac{(r^4 - r_1^4)}{4}\left[2\gamma_1 - \sin(\alpha+\beta)\cos(\alpha-\beta)\right] \qquad (5.108)$$

b. *Determination of the expression* $A_1(y_c^2 - y_1^2)$

Where A_1 is the area of the sector AOB.

$$A_1(y_c^2 - y_1^2) = r_1^2\gamma_1(y_c + y_1)(y_c - y_1) =$$

$$= r^2\gamma_1\left(\frac{4r\sin\gamma_1\sin\gamma_2}{3\gamma_1} + r\sin\beta\right)r\sin\beta =$$

$$= r^4\gamma_1\sin\beta\left(\frac{4\sin\gamma_1\sin\gamma_2}{3\gamma_1} + \sin\beta\right) \qquad (5.109)$$

c. *Determination of the expression* $A_2(y_{c1}^2 - y_3^2)$

Where A_2 is the area of the sector A_1OB_1.

$$A_2(y_{c1}^2 - y_3^2) = r_1^2\gamma_1(y_{c1} + y_3)(y_{c1} - y_3) =$$

$$= r_1^2\gamma_1\left(\frac{4r_1\sin\gamma_1\sin\gamma_2}{3\gamma_1} + r_1\sin\beta\right)r\sin\beta =$$

$$= rr_1^3\gamma_1\sin\beta\left(\frac{4\sin\gamma_1\sin\gamma_2}{3\gamma_1} + \sin\beta\right) \qquad (5.110)$$

The resulting value of the expressions (5.109) and (5.110) is

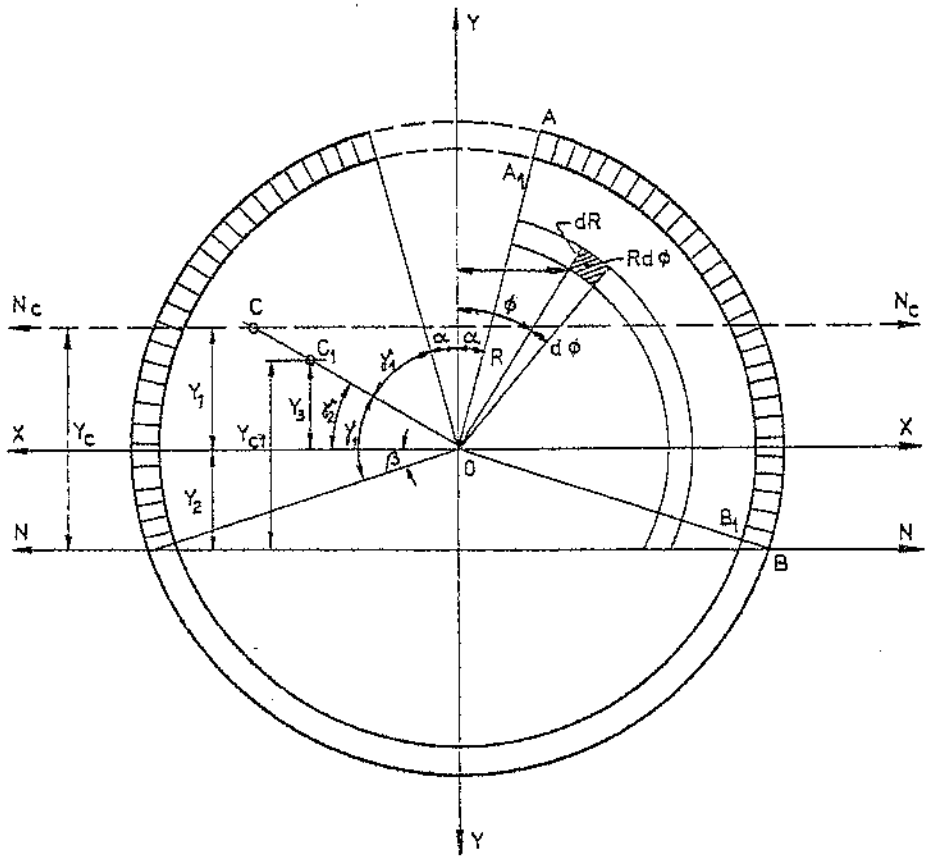

FIGURE 5.21 — Geometrical data for determination of moment of inertia of compressive area.

$$A_1(y_c^2 - y_1^2) - A_2(y_{c1}^2 - y_3^2) =$$

$$= r(r^3 - r_1^3)\gamma_1 \sin\beta \, x$$

$$x \left(\frac{4 \sin\gamma_1 \sin\gamma_2}{3\gamma_1} + \sin\beta \right) \qquad (5.111)$$

Therefore, total moment of inertia of compressed area with respect to the axis N-N is

$$I_c = \frac{(r^4 - r_1^4)}{4} \left[2\gamma_1 - \sin(\alpha+\beta) \cos(\alpha-\beta) \right] +$$

$$+ 2r(r^3 - r_1^3)\gamma_1 \sin\beta \left(\frac{4 \sin\gamma_1 \sin\gamma_2}{3\gamma_1} + \sin\beta \right) \qquad (5.112)$$

5.6.3.4 Moment of Inertia of the Tensile Area, Figure 5.22

Moment of inertia or ring EE_1GG_1 is with respect to the axis N-N is

$$I_N = I_{x_c} + Ay_N^2 \qquad (5.113)$$

Ordinate of centroid C of segment EFG is

$$y_c = \frac{4r \sin^3\phi}{3(2\phi - \sin 2\phi)} = \frac{4r \sin^3(90-\beta)}{3[2(90-\beta) - \sin 2\beta]} \qquad (5.114)$$

Moment of inertia of segment EFG with respect to ~~centroid axis $x_c - x_c$~~ is

Equation gives moment of inertia about centerline axis x-x

$$I_{x_c} = \frac{r^4}{8}(2\phi - \sin 2\phi)\left(1 + \frac{4 \sin^3\phi \cos\phi}{2\phi - \sin 2\phi}\right) \qquad (5.115)$$

Determination of the expression $A_1y_{N_1}^2$, where A_1 is the area of the segment EFG

$$A_1y_H^2 = \frac{r^2(2\phi - \sin 2\phi)}{2}(y_c - r\cos\phi)^2 =$$

$$= \frac{r^2(2\phi - \sin 2\phi)}{2}\left[\frac{4r \sin^3\phi}{3(2\phi - \sin 2\phi)} - r\cos\phi\right]^2 \qquad (5.116)$$

From (5.115) and (5.116), we obtain the expression for moment of inertia of segment EFG

$$I_1 = \frac{r^4}{8}\left[(2\phi - \sin 2\phi) + 4 \sin^3\phi \cos\phi\right] +$$

$$+ \frac{r^4}{2}(2\phi - \sin 2\phi)\left[\frac{4 \sin^3\phi}{3(2\phi - \sin 2\phi)} - \cos\phi\right]^2 \qquad (5.117)$$

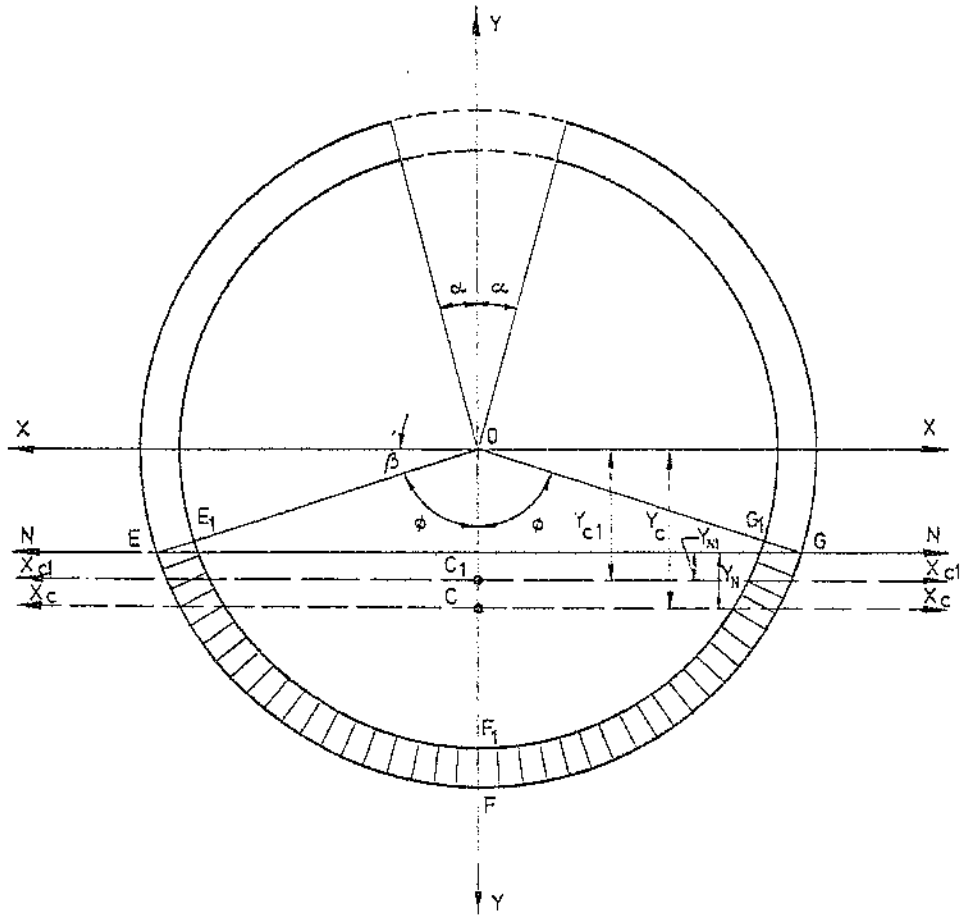

FIGURE 5.22 — Geometrical data for determination of moment of inertia of tensile area.

Moment of inertia of segment $E_1F_1G_1$ with respect to centroidal axis $x_{c_1} - x_{c_1}$

$$I_{c_1} = \frac{r_1^4}{8}(2\phi - \sin 2\phi)\left(1 + \frac{4\sin^3\phi\cos\phi}{2\phi - \sin 2\phi}\right) \tag{5.118}$$

Determination of the expression $A_2y_{N_1}^2$, where A_2 is the area of the segment EF_1G_1.

$$A_2y_{N_1}^2 = \frac{r_1^2(2\phi - \sin 2\phi)}{2}(y_{c_1} - r\cos\phi)^2 =$$

$$= \frac{r_1^2(2\phi - \sin 2\phi)}{2}\left[\frac{4r_1\sin^3\phi}{3(2\phi - \sin 2\phi)} - r\cos\phi\right]^2 \tag{5.119}$$

From (5.118) and (5.119), we obtain the expression for moment of inertia of segment $E_1F_1G_1$

$$I_2 = \frac{r_1^4}{8}\left[(2\phi - \sin 2\phi) + 4\sin^3\phi\cos\phi\right] + r_1^2\frac{(2\phi - \sin 2\phi)}{2}\left[\frac{4r_1\sin^3\phi}{2(2\phi - \sin 2\phi)} - r\cos\phi\right]^2 \tag{5.120}$$

Therefore, total moment of inertia of tensile area with respect to the neutral axis N-N is obtained by substructing from formula (5.117) the value (5.120), or

$$I_T = I_1 - I_2 = \frac{r^4}{8}\left[(2\phi - \sin 2\phi) + 4\sin^3\phi\cos\phi\right] + \frac{r^4}{8}(2\phi - \sin 2\phi)$$

2

$$\left[\frac{4\sin^3\phi}{3(2\phi - \sin 2\phi)} - \cos\phi\right]^2 -$$

$$- \frac{r_1^4}{8}\left[(2\phi - \sin 2\phi) + 4\sin^3\phi\cos\phi\right] -$$

$$- \frac{r_1^2(2\phi - \sin 2\phi)}{2}\left[\frac{4r_1\sin^3\phi}{3(2\phi - \sin 2\phi)} - r\cos\phi\right]^2 = \frac{(r^4 - r_1^4)}{8}\left[(2\phi - \sin 2\phi) + 4\sin^3\phi\cos\phi\right] + \frac{8}{9}(r^4 - r_1^4)\frac{\sin^6\phi}{(2\phi - \sin 2\phi)} -$$

$$- \frac{4}{3}r(r^3 - r_1^3)\sin^3\phi\cos\phi +$$

Derivation is not correct

$$+ \frac{r^2(r^2 - r_1^2)}{2}\cos^2\phi(2\phi - \sin 2\phi)$$

$$I_T = (r^4 - r_1^4)\left\{\frac{1}{8}\left[(2\phi - \sin 2\phi) + 4\sin^3\phi\cos\phi\right] + \frac{8}{9}\frac{\sin^6\phi}{(2\phi - \sin^2\phi)}\right\} -$$

$$- \frac{4}{3}r(r^3 - r_1^3)\sin^3\phi\cos\phi +$$

$$+ \frac{r^2(r^2 - r_1^2)}{2}\cos^2\phi(2\phi - \sin^2\phi) \tag{5.121}$$

After substituting $\phi = 90 - \beta$, we obtain

$$I_T = (r^4 - r_1^4)\left\{\frac{1}{8}\left[2(90-\beta) - \sin 2\beta + 4\cos^3\beta\sin\beta\right] + \frac{8}{9}\frac{\cos^6\beta}{2(90-\beta) - \sin 2\beta}\right\} -$$

$$- \frac{4}{3}r(r^3 - r_1^3)\cos^3\beta\sin\beta +$$

$$+ \frac{r^2(r^2 - r_1^2)}{2}\left[2(90 - \beta) - \sin 2\beta\right]\sin^2\beta \tag{5.122}$$

MecaStack does not follow the calculation for It presented due to the production of an incorrect value. MecaStack manually calculates It using sectors as Ic was calculated

5.6.4 Stresses at Breech Opening. Experimental Tests

In this chapter the effect of rectangular cutouts on the buckling of circular cylinder is discussed based on experimental investigations.

Because of the nonsymmetric nature of a cylinder with a cutout, analytical solutions for the buckling loads of such cylinders are difficult to obtain. This is especially true for large cutouts where nonlinearities become more pronounced. Consequently, studies of the effect of cutouts on the buckling of cylindrical shells have generally been limited to a few analytical solutions and to experimental tests.

Brogan and Almroth [5.56, 5.57] carried out a theoretical and experimental investigation of the effect of rectangular cutouts on the buckling loads of cylinders. The analysis was based on a two-dimensional finite-difference scheme, and this numerical solution entails treatment of a large system of nonlinear algebraic equations.

5.6.4.1 The Effect of Square and Rectangular Cutouts

The effects of square and rectangular cutouts on the buckling of cylinders loaded by central axial compression force are summarized by the results which are bounded by the curves shown in Figure 5.23.

Test cylinders had shell radius to thickness of the wall ratios $r/t = 400$. The dashed curve in Figure 5.23 repre-

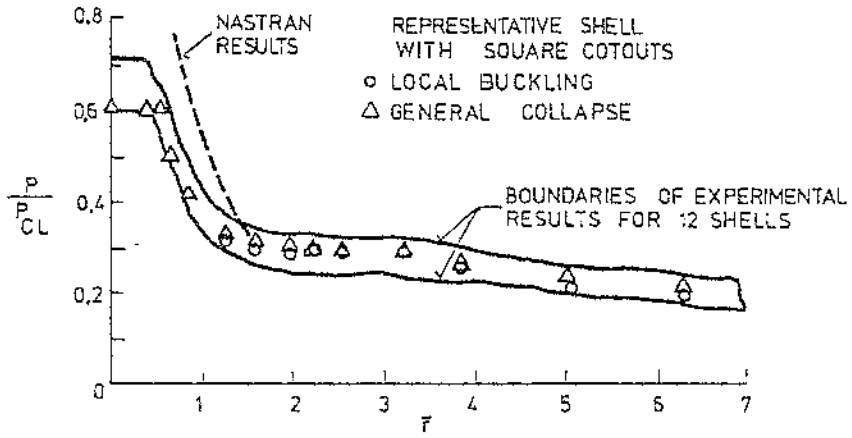

FIGURE 5-23 — The effect of square and rectangular cutouts on the buckling of circular cylinders loaded by central axial compression.

sents the results of a finite-element analysis. Most of the cylinders tested consisted of specimens with increasingly larger concentric square or rectangular cutouts in their sides. A limited number of cylinders had both square and rectangular cutouts with a common center.

The available prebuckling analyses are similar to that they all provide solutions that are dependent on a nondimensional geometric parameter

$$\bar{r} = \frac{r}{(Rt)^{\frac{1}{2}}} \qquad (5.123)$$

where

r = a characteristic hole dimension
R = the shell radius
t = the wall thickness

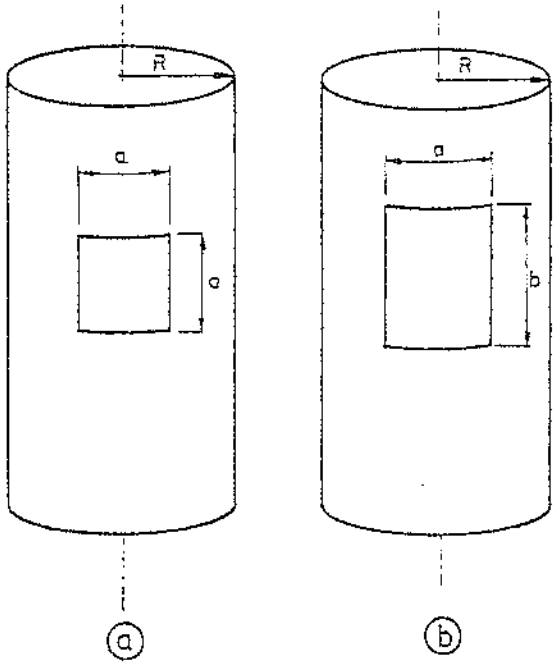

FIGURE 5.24 — Square and rectangular cuts in cylinders.

The characteristic hole dimension in the circulation parameter $\bar{r}$ is taken with reference to Figures 5.24 a and 5.24 b as follows:

The characteristic hole dimension as shown in Figure 5.24 a equal to one-half of the side length for the squares, or

$$\text{For } r = \frac{a}{2} \quad ; \quad \bar{r} = \frac{a}{2(Rt)^{\frac{1}{2}}} \qquad (5.124)$$

and for rectangular hole shown in Figure 5.24 b

$$\text{For } r = \frac{a+b}{4} \quad ; \quad \bar{r} = \frac{a+b}{4(Rt)^{\frac{1}{2}}} \qquad (5.125)$$

Even for such diversely different configurations as longitudinal and circumferential rectangles with aspect ratios equal to 2.0, all the experimental results for the cylinders with square and rectangular cutouts fill within the relatively narrow scatterband of Figure 3.1 when plotted with respect to r.

For values of $\bar{r}$ less than approximately 1.2, the buckling behavior of cylinders with square and rectangular cutouts was much the same as the behavior of cylinders with circular holes, Figure 5.25.

For values of $\bar{r}$ greater than about 1.2 the buckling loads continued to decrease with increasing $\bar{r}$, but at a much smaller rate of decline than that for the smaller values of $\bar{r}$.

For rectangular and square cutouts there was no transitional range as there was for circular cutouts, and the general collapse of the cylinders was always preceded by a stable local buckling made with an inward postbuckling deformation pattern.

For $\bar{r}$ between approximately 1.2 and 1.6, the stable local buckling mode always occurred in a symmetrical pattern approximately in the form of an ellipse with its semimajor axis tangent to the shell circumference. For $\bar{r}$ larger than about 1.6, the symmetrical stable local buckling mode was usually preceded by a nonsymmetrical mode aligned with one of the cutout diagonals which either snapped into its postbuckling form or just began growing inward as a larger local deformation.

For square and longitudinal rectangular cutouts with $\bar{r}$ greater than approximately 2.5, noticeable symmetric outward prebuckling deformations of the longitudinal

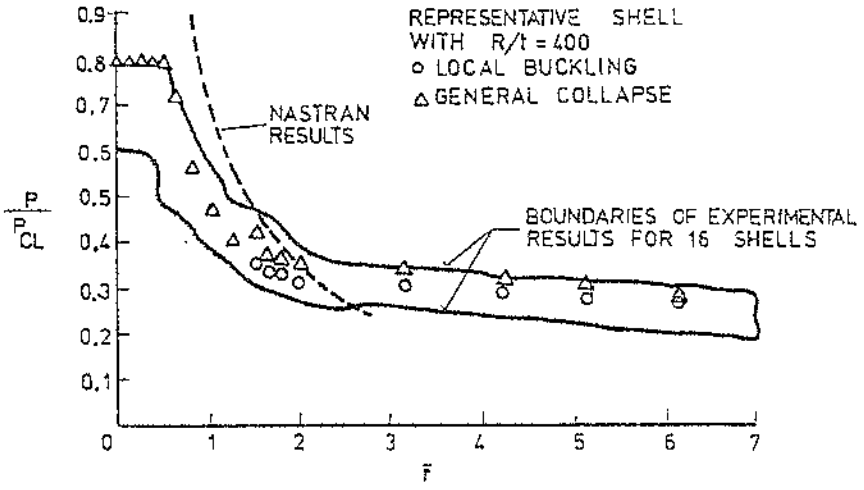

FIGURE 5.25 — The effect of circular cutouts on the buckling of circular cylinders loaded by central axial compression.

cutout sides preceded the above nonsymmetrical deformation.

For circumferential rectangles with $\bar{r}$ greater than about 3.2, noticeable symmetric outward prebuckling deformations of the circumferential cutout sides preceded the nonsymmetrical pattern. In all cases, the difference in the loads for the first noticeable local buckling and general collapse was small.

For $\bar{r}$ less than approximately 4.5, there was no detectable difference (beyond normal experimental scatter) between the general collapse loads for longitudinally and circumferentially oriented rectangles for the limited number of cylinders tested with each cutout configuration.

For $\bar{r}$ greater than 4.5, the general collapse loads of the circumferentially oriented rectangles tended to occupy the lower portion of the scatter bond in Figure 5.25. This phenomenon appears to be a result of the large prebuckling deformations and stable local buckling mode for the cylinder with circumferentially oriented rectangles which cause intensive stress redistribution to occur farther around the cylinder circumference.

Generally, for a given value of $\bar{r}$, the general collapse loads for cylinders with square and rectangular cutouts were found to be slightly lower than those for cylinders with circular cutouts. As an example, the difference in the general collapse loads for circular and square cutouts in the same cylinder are shown in Figure 5.26.

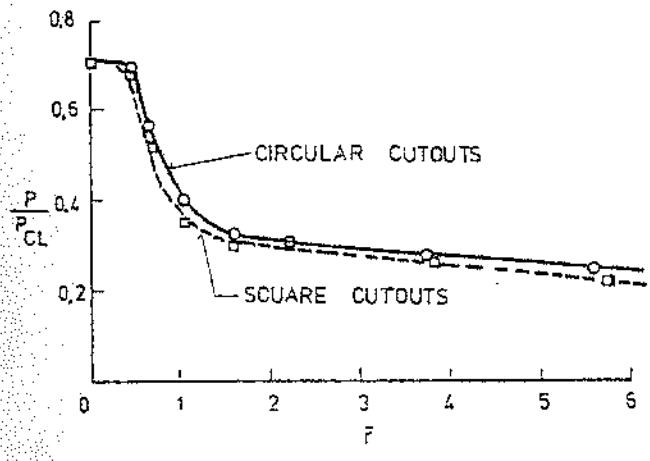

FIGURE 5.26 — The effect of circular and square cutouts on the buckling of a circular cylinder loaded by central axial compression.

5.7 Design of Stiffeners at Breech Opening

5.7.1 Design of Vertical Stiffeners

In order to avoid eccentric loading and a change in the direction of the stress, it is necessary to keep the neutral axis throughout the compensated cross-section on the centre line of the whole stack. It should be noted that it is not easy to obviate some of the eccentric loading on the compensating members. Such eccentric loading is offset in part by the fact that the line of action of the loading in the stack plates above and below the breech opening is often as far from the centre line of the stack, as the neutral axis of its compensating member.

The statical moment of the removed plate, where 2α is the angle in radians subtended at the stack center by the arc removed, Figure 5.27, is

$$S_x = \int_{-\alpha}^{+\alpha} (tR d\alpha)\ R\cos\alpha = 2tR^2\sin\alpha \qquad (5.126)$$

Using two vertical stiffeners, we may determine the required cross-sectional area of each stiffener by equalizing statical moments of the cross-sectional areas of the stiffeners $2A_s$ and the removed part of the stack, or

$$2A_s\bar{d} = 2tR^2\sin\alpha \qquad (5.127)$$

from which

$$A_s = \frac{tR^2\sin\alpha}{\bar{d}} \qquad (5.128)$$

where $\bar{d}$ is the distance between the centroid of cross-section of stiffener and axis x-x of the stack.

5.7.1.1 The Load Imposed on Each Stiffener by Steel Shell and Lining

$$G = \frac{\pi dH}{360} \left(D_s t_s \rho_s + D_\ell t_\ell \rho_\ell\right) \qquad (5.129)$$

where

G = total load on single stiffener

D_s, D_ℓ = inside diameter of the stack and lining, respectively

t_s, t_ℓ = the thickness of the wall and lining, respectively

ρ_s, ρ_ℓ = specific weights of the steel and lining materials, respectively

H = height of the stack above the breech opening

The axial compressive stress in each stiffener, under the weight of the wall and lining above the breech opening is

$$f_G = \frac{G}{A_s} = \frac{\pi dH}{tR^2 \sin\alpha} \left(\frac{\alpha}{360}\right)\left(D_s t_s \rho_s + D_\ell t_\ell \rho_\ell\right) \qquad (5.130)$$

5.7.1.2 The Load Imposed on Each Stiffener Due to Wind Bending Moment

Compressive stress in the stack's wall due to the wind load moment is

$$\sigma_w = \frac{4M_w}{\pi D_m^2 t} \qquad (5.131)$$

where

M_w = bending moment due to wind load

D_m = mean diameter of the stack at cross-section under consideration

Cross-sectional area of the wall of the stack is

$$\pi D_m t \qquad (5.132)$$

Therefore, the approximate load imposed on each stiffener is

$$P_w = \frac{4M_w}{\pi D_m^2 t} \times \pi D_m t \times \frac{\alpha}{360} = \frac{M_w \alpha}{90\ D_m} \qquad (5.133)$$

and the axial compressive stress in each stiffener under the wind pressure on the stack is

$$f_w = \frac{P_w}{A_s} = \frac{M_w \alpha}{90\ D_m} \times \frac{4d}{tD_m^2 \sin\alpha} = \frac{M_w d\alpha}{22.5\ tD_m^3 \sin\alpha} \qquad (5.134)$$

5.7.1.3 The Eccentric Bending Moment Due to Eccentricity of Stiffener

By designating the distance between wall and centroid of the cross-section of the stiffener "e", the eccentric bending moment due to the loads $(G + P_w)$ is

$$M_e = (G + P_w)e \qquad (5.135)$$

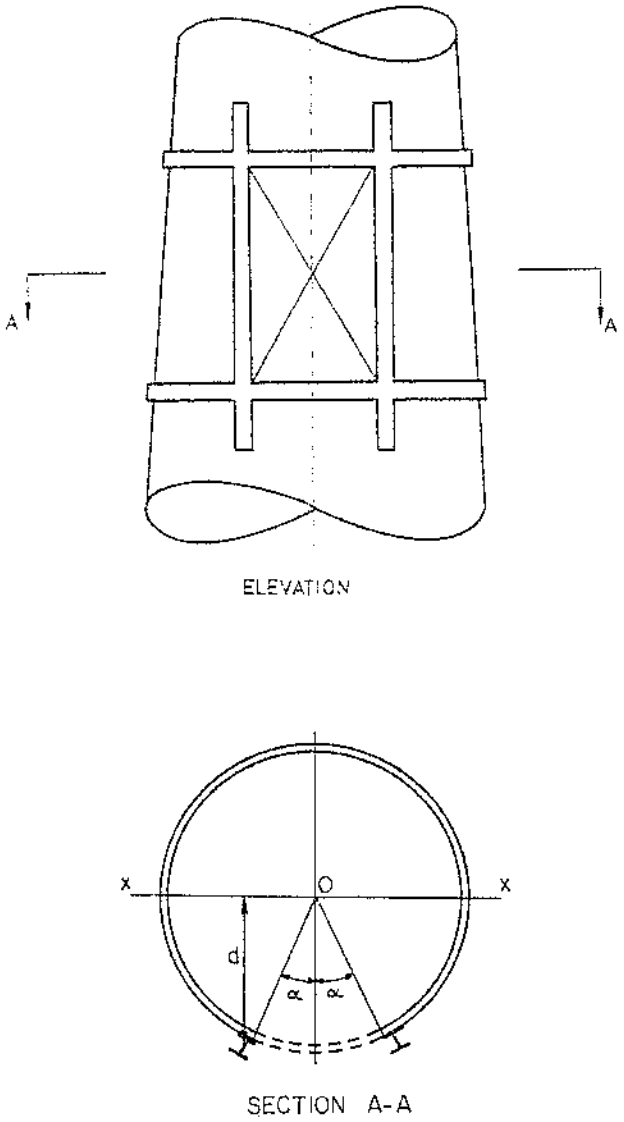

FIGURE 5.27 — Breech opening geometry.

and corresponding axial stress is

$$f_e = \frac{(G + P_w)e}{S_{stiff}} \qquad (5.136)$$

where S_{stiff} is section modulus of the stiffener cross-section.

Total axial stress is

$$f_{tot} = f_G + f_w + f_e \qquad (5.137)$$

5.7.1.4 The Effect of the Stiffened Breech Opening on the Strength of the Stack

To evaluate this effect it is necessary to determine the moment of inertia of the removed area of the arc with respect to the stack center line, as follows, Figure 5.28.

The moment of inertia of the area of the arc removed about a stack center line is

$$I_{rem} = t\int_{-\alpha}^{\alpha} R^3\cos^2\alpha d\alpha = R^3\left(\alpha + \frac{\sin 2\alpha}{2}\right)t \quad (5.138)$$

The approximate moment of inertia of the stiffener cross-section with respect to the stack center line is

$$I_{stiff} = A_s d^2 \quad (5.139)$$

where

A_s = cross-sectional area of the stiffener

d = distance between the center of gravity of the cross-section of stiffener and axis x-x.

Assuming

$$2I_{stiff} > I_{rem} \quad (5.140)$$

then

$$2I_{stiff} - I_{rem} = 2A_s d^2 - I_{rem} = \Delta I \quad (5.141)$$

where ΔI is an increase in the moment inertia of removed part of the cross-section of the stack.

The moment of inertia of the original cross-sectional area of the stack is I, therefore the compensated value is

$$I + \Delta I \quad (5.142)$$

By designating the distance between the extreme edge of the stiffener and center of the stack as d_1, Figure 5.28, the section modulus of the cross-section of the stack is

$$S_{stiff} = \frac{I + \Delta I}{d_1} \quad (5.143)$$

Assuming that

$$S_{orig} > S_{stiff} \quad (5.144)$$

Therefore, the reduction in section modulus of stiffened cross-section of the stack in % is

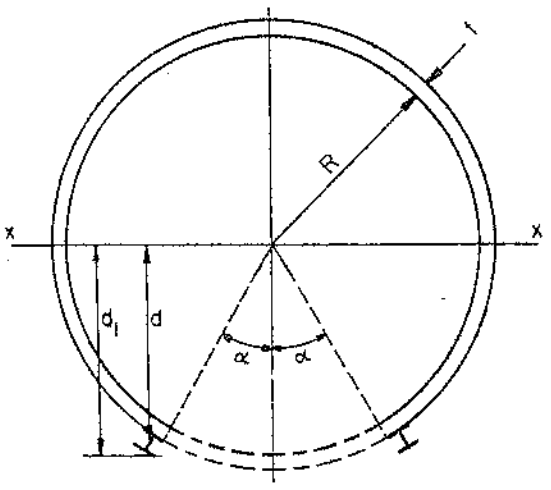

FIGURE 5.28 — Breech opening and stiffeners geometry.

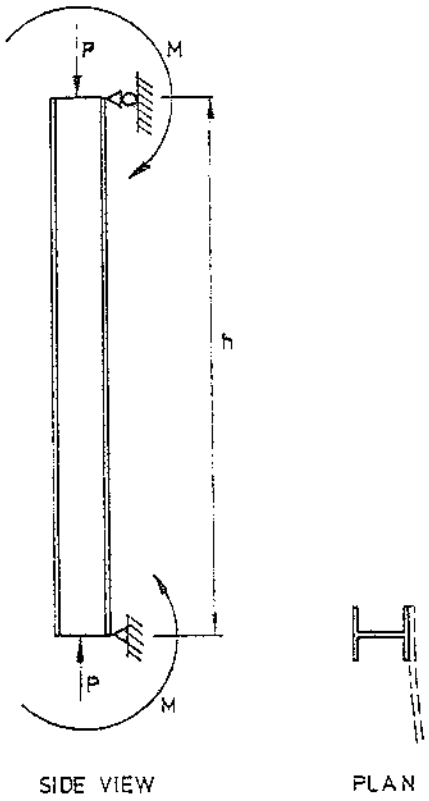

FIGURE 5.29 — Vertical stiffener as beam-column.

$$\frac{S_{stiff}}{S_{orig}} \times 100\% \quad (5.145)$$

It should be remembered, however, that the stress in the extreme edge of the stiffener is

$$f_{stiff} = \frac{\Sigma M}{S_{stiff}} \quad (5.146)$$

whereas the stress in the stack plates themselves is actually lessened in the ratio

$$\frac{I}{I + \Delta I} \quad (5.147)$$

or, the original moment of inertia divided by the new moment of inertia. Thus, the original section modulus is not seriously weakened, and the plate stress is reduced.

5.7.1.5 Buckling Stability of Vertical Stiffeners

Vertical stiffeners under action of axial load and bending moments due to the eccentricity of axial loads at both ends, may be considered as beam-columns. To achieve the greater factor of safety, the stiffeners will be considered as isolated beam-columns, neglecting the plating of the wall to which the stiffeners are connected. Both ends of the stiffeners are assumed as hinges, Figure 5.29.

The maximum stress at mid length of the column is given by the secant formula [5.58]

$$\sigma_{max} = \frac{P}{A} + \frac{M_o c}{I}\sec\frac{h}{2}\sqrt{\frac{P}{EI}} \quad (5.148)$$

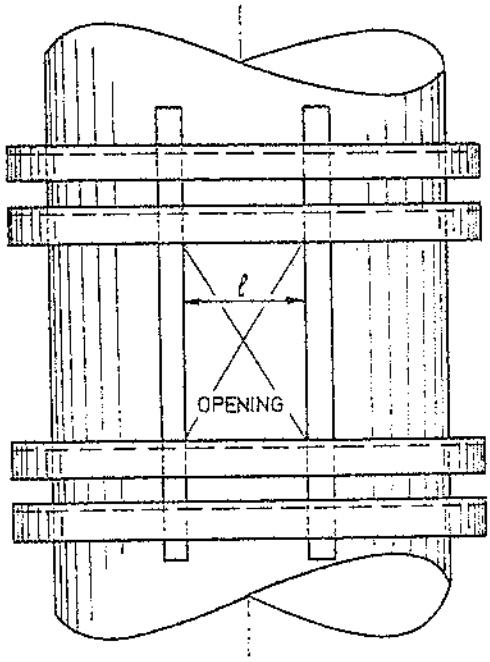

FIGURE 5.30 — Ring girders.

5.7.2 Ring Stiffeners

In addition to the compensation members which are placed as vertical stiffeners, horizontal reinforcement should be provided by using ring girders above and below the breech opening. These ring stiffeners should be designed as beams fixed to the wall of the stack to carry the unsupported parts of the stack above and below breech opening, Figure 5.30.

The span in bending is the width between the vertical stiffeners, but the girder should encircle the stack to preserve circularity at the opening.

To form each ring girder, steel plates should be placed to act as top and bottom flanges. The shell of the stack can serve as a web.

Around the stack, each ring girder must be capable of carrying a uniformly distributed load lb/in of arc due to axial vertical load

$$w_1 = \frac{G}{2\pi R} \tag{5.149}$$

and due to the wind bending moment, when the stress is

$$f = \frac{M_w}{\pi R^2 t} \tag{5.150}$$

Therefore, the corresponding vertical load is

$$ft = w_2 = \frac{M_w}{\pi R^2} \tag{5.151}$$

The total distributed load in lb/in

$$w = w_1 + w_2 = \frac{G}{2\pi R} + \frac{M_w}{\pi R^2} \tag{5.152}$$

The bending moment in the girder is

$$M = \frac{w\ell^2}{12} = \frac{\ell^2}{12\pi R}\left(\frac{G}{2} + \frac{M_w}{R}\right) \tag{5.153}$$

5.8 Rigorous Breech Opening Analysis

Ever since the advent of plate structures, the structural arrangements in the vicinity of openings in them have been a matter of considerable concern.

When analyzing and designing such structures, various factors have to be taken into consideration. One of these is the "stress concentration" around openings, recesses and cutouts in plane and three dimensional parts of structures.

The initial theoretical work on this subject was performed by Inglis [5.59] who approximate the effect of a rectangular opening with rounded corners by a pair of ellipses intersecting obliquely. Savin [5.60] studied both the square and the rectangle openings with rounded corners. Greenspan [5.61] working independently and by another method, produced a solution for the square with rounded corners. None of these analytical approaches is applicable to a wide variety of rectangular openings. The first step to rectify this situation was taken by Brock [5.62] who presented a solution for the entire family of rectangles with rounded corners.

An outstanding theoretical study of stresses around rectangular openings in cylindrical shells appears by Muskhelishvili [5.63]. He makes use of the complex-variable method in conjunction with conformal mapping technique in investigating such a problem. His solution is based on the assumptions of plane elasticity: homogeneous, isotropic material within the elastic limit, uniform stress across the thickness of the shell with no stress normal to it, an opening "small" relative to the shell and "small" displacements.

An accurate analysis of the stresses around openings in stacks until recently has been beyond the state of the art in shell analysis. The large number of parameters involved makes in impossible to produce design charts for designing reinforcement around openings by use of a purely empirical approach and a theoretical analysis has been prohibited by the lengthy and complicated mathematics involved. Consequently, design of opening reinforcement has been based on rules of thumb which are generally quite conservative due to the uncertainty involved. However, recent advances in the Finite Element Method of Analysis coupled with improvements in computer technology and numerical analysis methods have brought the state of the art to a level where it now appears feasible to establish design procedures with a more solid foundation [5.64, 5.65, 5.66, 5.67, 5.68].

5.8.1 The Finite Element Program

The invention of digital computers has significantly improved the output of engineering profession. Manual methods were the only means of performing engineering calculations up to the end of the Second World War. They were not practical because of the enormous calculation work involved in solving a large number of simlutaneous equations encountered in analyzing any reasonably large structure. To overcome this difficulty, engineers resorted to comparatively easier but approximate methods, e.g. relaxation and successive approximation methods. These methods, though still in use at present, have been virtually replaced by computerized stiffness solution methods –

incorporating the finite element technique and matrix methods for structural analysis [5.69].

Computers seem to be ideally suited for modern structural analysis problems because of their versatility and tremendous speed resulting in substantial savings in time and man-hours required for a particular project. In addition, computer programs using finite elements have the following distinct advantages:

1. Their ability to use elements of various types, sizes and shapes and to model a structure of arbitrary geometry.
2. Their ability to accommodate arbitrary support conditions and arbitrary loading, including thermal loading.
3. Their ability to model composite structures involving different structural components such as stiffening members and a shell and combination of plates, bars and solids, etc.
4. The finite element structure closely resembles the actual structure instead of being quite a different abstraction that is hard to visualize.

Invariably, the finite element method of analysis entails a few disadvantages as well, as shown below:

1. A specific numerical result is obtained for a specific problem. A general close form solution, which would permit one to examine system response to changes in various parameters, is not produced.
2. Experience and judgement are needed in order to construct a good finite element model.
3. A large computer and a reliable computer program are essential.
4. Input and output data may be large and tedious to prepare and interpret.

5.8.2 Method of Finite Element Analysis

Finite element analysis has come about through the use of digital computers solving with matrix algebra methods the many equations of compatibility and equilibrium created by classical solution techniques such as slope deflection. Generally, most finite element analysis programs utilize displacement methods of solution, resolving deflections first, followed by a stressing routine, which solves for member forces (stresses) from the deflections -- i.e., a stiffness solution method [5.70, 5.71].

What must be appreciated, however, is the fact that all finite element models are at best approximations of the actual structures they may represent. Firstly, the applicability of finite element analysis must be determined with respect to a problem in hand. If it is possible to model an actual structure under consideration, it then becomes necessary to carefully choose a proper element and grid pattern such that the errors, that incur when the actual structural continuum is replaced by the finite element model, may be minimized. Furthermore, though must be used to establish the appropriate constraints that must be applied about the model so that the model and actual structure tend to behave similarly.

Over the past years, as finite element technology grew, its popularity also increased. Subsequently, at the moment, good evidence exists verifying the viability of the finite element analysis method as quite reliable when applied properly.

Generally speaking the steel stack analyzed in this report is well ordered and no a complex problem to solve. It is anticipated that the results of the analysis presented in Appendix B, are very reflective of the forces and deflections that would exist if the modelled structure and the applied loads were in actual existence.

5.8.3 ANSYS Computer Program

ANSYS is a large scale general purpose computer program for the solution of several classes of engineering analysis problems. Its analyzing capabilities include static and dynamic; plastic, creep and swelling; small and large deflections; steady state and transient heat transfer and steady state fluid flow.

The matrix displacement method of analysis based upon finite element idealization is employed throughout the program. The library of finite elements available numbers more than forty for static dynamic analyses and ten for heat transfer analyses. This variety of elements gives the ANSYS program the capability of analyzing frame structures (two dimensional frames, grids and three dimensional frames), piping systems, two dimensional plane and axisymmetric solids, flat plates, three dimensional solids, axisymmetric and three dimensional shells and nonlinear problems including interfaces and cables.

Loading on the structure may be forces, displacements, pressures, temperatures or response spectra. Loading may be arbitrary time functions for linear and nonlinear dynamic functions for linear and nonlinear dynamic analyses. Loadings for heat transfer analyses include internal heat generation, convection and radiation boundaries, and specified temperatures or heat flows [5.72].

The ANSYS program uses the wave front (or "frontal") direct solution method for the system of simultaneous linear equations developed by the matrix displacement method, and gives results of high accuracy in a minimum of computer time. The program has the capability of solving large structures. There is no limit on the number of elements used in a problem. The number of nodes can be in excess of 2500 for three dimensional problems, and 5000 for two dimensional problems. There is no "band width" limitation in the problem definition, however, there is a "wave front" restriction. The "wave front" restriction depends on the amount of core storage available for a given problem. Up to 576 degrees of freedom on the wave front limitation tends to be restrictive only for analysis of arbitrary three dimensional solids or in the use of ANSYS on a small computer.

ANSYS has the capability of generating substructures (or super-elements). These substructures may be stored in a library file for use in other analyses. Substructuring portions of a model can result in considerable computer time savings for nonlinear analyses.

Geometry plotting is available for all elements in the ANSYS library, including isometric, perspective and section views of three dimensional structures. Plotting subroutines are also available for the plotting of stresses and displacements from two and three dimensional solid or

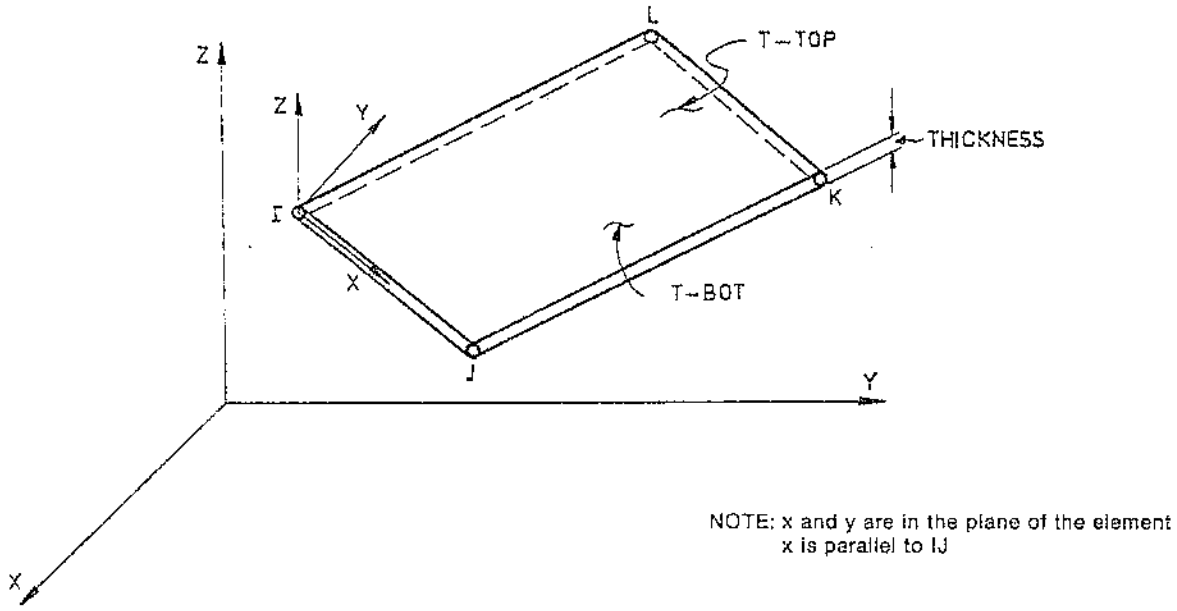

FIGURE 5.31 — Flat quadrilateral shell element.

shell analyses, node shapes from dynamic analyses, distorted geometries from static analyses, transient forces and displacements vs. time curves from transient dynamic analyses, and stress strain plots from plastic and creep analyses.

Post processing routines are available for algebraic modification, differentiation, and integration of calculated results. Root mean square operations may be performed on seismic modal results. Results from various loading nodes may be combined for harmonically loaded axisymmetric structures.

Options for multiple coordinate system in cartesian, cylindrical, or spherical coordinates are available, as well as multiple region generation capabilities to minimize the input data for repeating regions.

Sophisticated geometry generation capabilities are included for two dimensional plane and axisymmetric structures and for intersecting three dimensional shell structures [5.73, 5.74].

The quadrilateral shell element has bending and membrane capabilities. Both in-plane and normal loads are permitted. The element has six degrees of freedom at each node: translation in the nodal x, y, and z directions and rotations about the nodal x, y, and z axes. Figures 5.31 and 5.32.

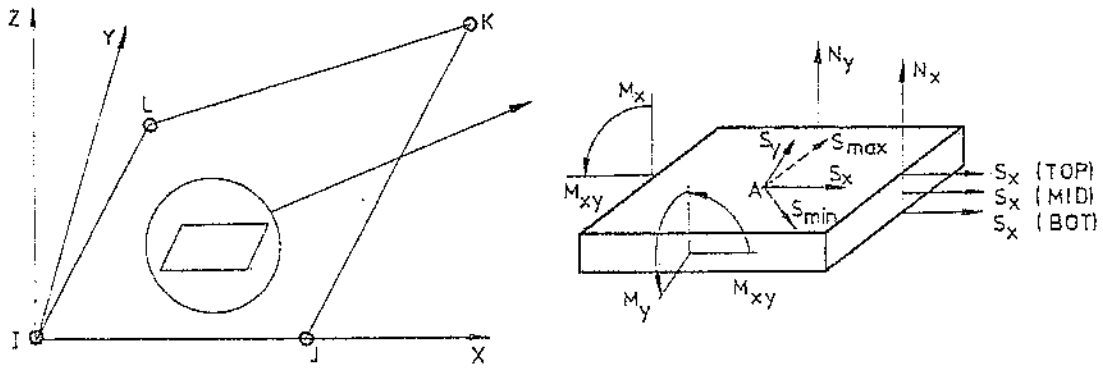

FIGURE 5.32 — Flat quadrilateral shell element output.

NUMERICAL EXAMPLE NO. 1
Approximate Method

Determine stresses and design stiffeners at breech opening of self-supported steel stack to prevent buckling under vertical and wind loading, Figure 5.33.

Assumed

Location: Toronto, Ontario

Material: C.40.21 50 A (equivalent ASTM Steel)
This is weathering steel and although more expensive than 44W, a saving will be made due to lower maintenance costs.

Height Required: 200 ft.

Minimum Discharge Diameter: 10 ft.

Corrosion Allowance: 1/16 inch

Solution

1. Part 1. Determination of Wind Loading

From NBC, Supplement No. 1, 1975, p. 43, the hourly wind pressure for Toronto is 9.9 psf at 1 in 30.

Check $\frac{L}{D}$ ratio: $\frac{L}{D} = \frac{200}{13} = 15.4$

where $D = \frac{D_t + D_b}{2} = \frac{10 + 16}{2} = 13$ ft.

Since $\frac{L}{D} < 100$, Figure B-11, p.77 must be considered.

From Figure B-11, for L/D = 15.4, Cn = 0.65
According to NBC, p. 157
The gust effect factor for structured members is C_g = 2.0.
The exposure factor Ce from NBC, Supplement No. 4, p. 56, is

$$C_e = 0.6 \left(\frac{H}{50}\right)^{\frac{1}{2}}, \quad C_e > 0.5$$

Total force, Fn, NBC Supplement 4, p. 77 is

$$F_n = C_n q \, C_g \, C_e \, A_c$$

C_e and A_c are functions of H_X, i.e., the height of the stack at a point x from the top as shown in Figure 5.33. Therefore,

$$F_n = 0.65 \ (9.9) \ (0.6) \left[\frac{H_X}{60}\right]^{\frac{1}{2}} (2.0) \left(16 - \frac{6H_X}{200}\right)$$

a. Wind pressure from 0 to 40 ft (exactly 0 to 41'-8").
The exposure factor C_e = 0.50

$$F_n = 0.65 \times 9.9 \times 0.5 \times 2.0 \left(16 - \frac{6H_X}{200}\right) =$$

$$= 103 - 0.193 \, H_X$$

b. Wind pressure from 40 to 200 ft.

$$F_n = 0.65 \times 9.9 \times 0.6 \left(\frac{H_X}{60}\right)^{\frac{1}{2}} 2.0 \left(16 - \frac{6H_X}{200}\right) =$$

$$= (15.95 - 0.03 \, H_X) \sqrt{H_X}$$

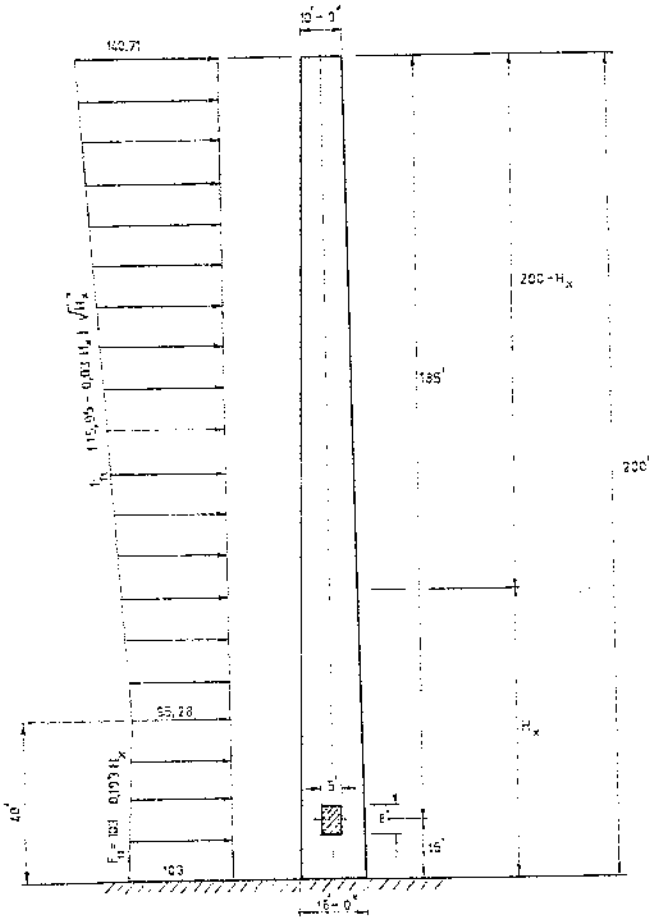

FIGURE 5.33 — Distribution of wind load acting on the stack.

For

H_X = 0	F_n = 103
H_X = 40	F_n = 95.28
H_X = 200	F_n = 140.71

2. Part 2. Bending Moments

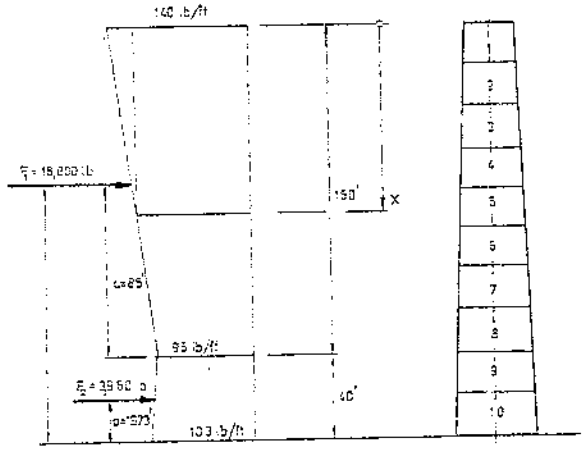

FIGURE 5.34 — Determination of bending moments in stack under wind loading.

Mx for uniform loading if x < 160'-0"

$$M_{xu} = \left[\frac{45(160 - x)}{160} + 95\right]\frac{x^2}{2} = (70 - 0.1406x)x^2$$

Mx for triangular loading if x > 160'-0"

$$Mxt = 0.0938x^3$$

Total moment when x < 160'-0"

$$M_x = (70 - 0.1406x)x^2 + 0.0938x^3 = 70x^2 - 0.0468x^3$$

For the bottom part x > 160'-0" the exact expression is

$$M_x = \frac{(0.1x^2 + 63x - 12640)(x - 160)(0.2x + 253)}{3(0.2x + 158)}$$

However, for the bottom 40 ft. the wind loading can be considered to be uniform and set equal to 95 lb/ft, or

$$M_x = \frac{95(x - 160)^2}{2} = 47.5(x - 160)^2$$

Moment at the base

$$F_1 = \frac{1}{2}(95 + 140)\,160 = 18800 \text{ lbs}$$

$$a = \frac{160(2 \times 140 + 95)}{3(140 + 95)} = \frac{160 \times 375}{3 \times 235} = 85 \text{ ft}$$

$$M_{F_1} = 18800 \times (85 + 40) = 2{,}250{,}000 \text{ lb/ft} = 28{,}200{,}000 \text{ lb/in}$$

$$F_2 = \frac{1}{2}(95 + 103)\,40 = 3960 \text{ lbs}$$

$$a_1 = 40 - \frac{40(2 \times 103 + 95)}{3(103 + 95)} = 19.73 \text{ ft}$$

$$M_{F_2} = 3960 \times 19.73 = 78130.8 \text{ lb/ft} = 937{,}570 \text{ lb/in}$$

$$M_{tot} = 28{,}200{,}000 + 937{,}570 = 29{,}137{,}570 \text{ lb/in}$$

3. Part 3. Determination of Stack's Wall Thickness

In order to determine the required thickness of stack's wall, the moment due to wind should be determined. The critical buckling stress can be determined from equations:

$$f_s = \frac{W_s}{\pi D_i (t-c)}$$

$$f_w = \frac{4M_w}{\pi D_1^{\,2}(t-c)}$$

Combining both of the above equations and substituting $\sigma_{cr} = f_s + f_w$ yields

$$\sigma_{cr} = \frac{W_s}{\pi D_i (t-c)} + \frac{4M_w}{\pi D_i^2 (t-c)}$$

setting t' = t-c, the equation can be rearranged so that t can be optimized. Therefore,

$$t' = \frac{W_s}{\pi \sigma_{cr} D_i} + \frac{4M_w}{\pi \sigma_{cr} D_i^{\,2}}$$

Assume t' = 0.50 inch at base

Therefore $\frac{D}{t'} = \frac{16 \times 12}{0.5} = 384$

Since $\frac{D}{t} < 400$, the Wilson-Newmark equation cannot be used, therefore, the AISI formula applies.

Since $\frac{13000}{F_y} = 260 < \frac{D}{t'}$,

$$\sigma_{cr} = \frac{5333}{D/t'} = 13.9 \text{ ksi}$$

To determine the approximate own weight of the stack, assume upper 100 ft thickness of the wall ¼ in. and bottom 100 ft. wall having ½ in. wall thickness

$$W_s = \frac{\pi D \times t \times 490 \times 100}{12}$$

$$W_s = \frac{49000 \times 3.14}{12}\left(\frac{10 + 13}{2} \times \frac{1}{4} + \frac{13 + 16}{2} \times \frac{1}{2}\right) =$$

$$= 12821.66\,(2.875 + 7.25) = 129819.31 \approx 130{,}000 \text{ lbs}$$

And

$$t_1 = \frac{130{,}000}{13900(16 \times 12)\pi} \times \frac{4 \times 29{,}137{,}570}{13{,}900(16 \times 12)^2 \pi} =$$

$$= 0.0155 + 0.0724 = 0.0879 \text{ in}$$

From this preliminary check it can readily be seen that the stress at the bottom of the stack is not critical.

In addition, the deflection of the stack must be considered when determining the required thickness of the stack. According to the British Standard for the design of Steel Chimneys, the maximum allowable deflection at the top of steel stack is

$$\Delta = \ell/200$$

The maximum permissible deflection at the top of this stack should therefore be

$$\Delta = 200/200 = 1 \text{ ft}$$

The actual deflection will be found using the method of virtual work, or

$$1 \text{ lb} \times \Delta = \int_0^L \frac{m\,M dx}{EI}$$

or

$$\Delta_{tot} = \sum \Delta_i = \sum_{i=1}^{10} \frac{m_i M_i \Delta x}{E I_i}$$

where

m = moment at x due to 1 lb load applied at top of stack

M_i = moment on segment i due to wind loading

I_i = $\pi D_i\, t/8$ = moment of inertia of segment i at its centroid, which for this example will be considered at ½ the height of the segment

Maximum allowable deflection at top of stack is 12 inches.

Calculated deflection at top is

$$10.794 < 12 \text{ inches}$$

therefore actual deflection is less than allowable.

4. Part 4. Determination of the Own Weight of Stack and Wind Bending Moment

a. Own Weight of the Stack above Breach Opening

Diameter $D_2 = 120 + 0.36x = 120 + 0.36 \times 90 = 152.4'' =$
$= 12'\text{-}8.4''$

Diameter $D_3 = 120 + 0.36 \times 185 = 186.6'' = 15'\text{-}6.6''$

$$P_1 = \frac{\pi \times 490 \times 90}{12} \left(\frac{D_1 + D_2}{2} \times t\right) =$$

$$= \frac{3.14 \times 490 \times 90}{12} \left(\frac{10 + 12.7}{2} \times \frac{1}{4}\right) =$$

$= 23{,}743$ lbs

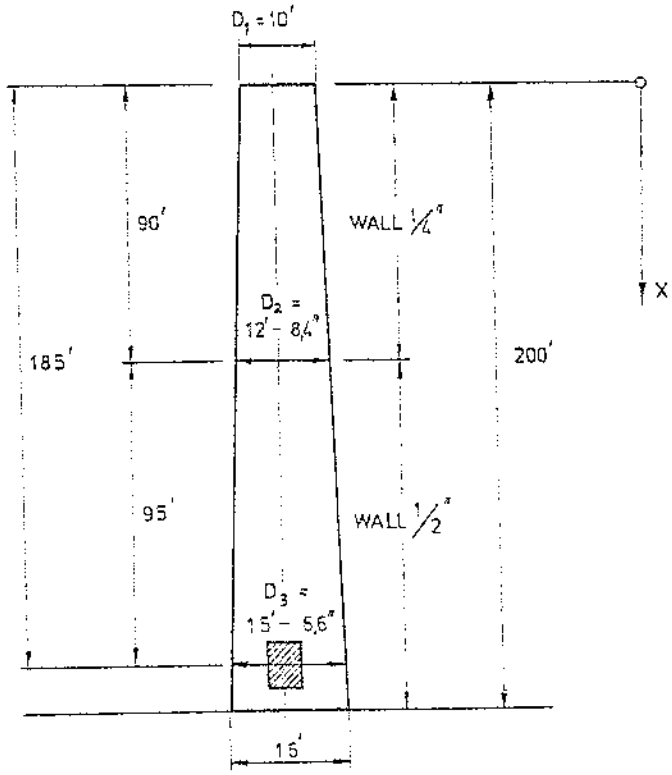

FIGURE 5.35 — Stack's wall dimensions.

$$P_2 = \frac{\pi \times 490 \times 90}{12} \left(\frac{12.7 + 15.55}{2} \times \frac{1}{2}\right) =$$

$= 81{,}498$ lbs

Total $P = P_1 + P_2 = 114{,}768$ lbs

TABLE 5.6 — Deflections of Stack.

SEC No.	Diameter (in)	x (ft)	m (in-lb)	Mi (in-lb)	m Mix / E	t' (in)	I=πd³t'/8 (in)	Δtop (in)
(1)	(2)	(3)	(4)	(5)	(6)	(7)	(8)	(9)
1	123.6	10	120	83,438	4	¼	185,375	0.015
2	130.8	30	360	740,832	3,200	¼	219,700	0.015
3	138.0	50	600	2,029,800	24,358	¼	258,000	0.094
4	145.2	70	840	3,923,400	92,278	¼	300,540	0.307
5	152.4	90	1080	6,394,680	248,625	¼	347,500	0.715
6	159.6	110	1320	9,416,520	546,911	½	792,200	0.685
7	166.8	130	1560	12,962,160	1,051,490	½	911,200	1.154
8	174.0	150	1800	17,004,600	1,836,496	½	1,034,400	1.775
9	181.2	170	2040	21,516,840	2,984,816	½	1,178,160	2.555
10	188.4	190	2280	26,472,000	4.587,068	½	1,313,000	3.494
d = 12 + 0.36x, in. where x(ft)					Total deflection = Δtop = 10.794			

b. Determination of the Bending Moment under Wind Load at x = 185 ft., Fig. 5.34

$M_1 = 18{,}800 \times (85 + 25) \times 12 = 24{,}816{,}000$ lb/in

$M_2 = \frac{95}{2} \times (185 - 160)^2 \times 12 = 356{,}250$ lb/in

Total $M_W = 24{,}816{,}000 + 356{,}250 = 25{,}172{,}250$ lb/in

5. Part 5. Determination of Cross-Section Statical Properties

a. Statical Moment of the Compressed Area; Figure 5.36
Assume the position of the neutral axis as shown in Figure 5.36, y_c = in. yc = 36 in {Omitted from Text}
According to formula (5.96)

$$S_c = \frac{4}{3}(r^3 - r_1^3)\sin\gamma_1 \sin\gamma_2 + 2r(r^2 - r_1^2)\gamma_1 \sin\beta$$

where $\alpha = 18^\circ 50'$

$\sin\beta = \frac{36}{93} = 0.3871$; $\beta = 22^\circ 50'$

$\gamma_1 = \frac{90 - \alpha + \beta}{2} = \frac{94}{2} = 47^\circ$;

$\gamma_1(\text{rad}) = \frac{47}{57.296} = 0.8203$

$\gamma_2 = \frac{90 - \alpha - \beta}{2} = \frac{48^\circ 20'}{2} = 24^\circ 10'$

$\sin\gamma_1 = \sin 47^\circ = 0.7314$

$\sin\gamma_2 = \sin 24^\circ 10' = 0.4094$

$S_c = \frac{4}{3}(93^3 - 92.5^3) \times 0.7314 \times 0.4094 + 2 \times 93 (93^2 - 92.5^2) \times 0.8203 \times 0.3871 = \frac{4}{3} \times 12904 \times 0.2994 + 186 \times 92.75 \times 0.3175 =$

$= 5138 + 5478 = 10{,}616$ in^3

b. Statical Moment of the Tensile Area, Figure 5.36
According to formula (5.103)

$$S_T = \frac{2}{3}(r^3 - r_1^3)\cos^3\beta - \frac{r}{2}(r^2 - r_1^2)[2(90-\beta) - \sin 2\beta]\sin\beta$$

where

$\frac{2(90-\beta)}{57.296} = \frac{2(90-22^\circ 50')}{57.296} = \frac{134.333}{57.296} = 2.3445$

$\sin 2\beta = \sin 45^\circ 40' = 0.7153$

$\cos\beta = \cos 22^\circ 50' = 0.9216$

$S_T = \frac{2}{3}(93^3 - 92.5^3)\,0.9216^3 - \frac{93}{2}(93^2 - 92.5^2) \times [2.3445 - 0.7153] \times 0.3871 =$

$= \frac{2}{3} \times 12904 \times 0.7828 - 46.5 \times 9275 \times 1.6293 \times 0.3871 = 6735 - 2720 = 4{,}015$ in^3

c. Moment of Inertia of the Compressed Area
According to formula (5.112)

$$I_c = \frac{(r^4 - r_1^4)}{4}[2\gamma_1 - \sin(\alpha+\beta)\cos(\alpha-\beta)] + 2r(r^3 - r_1^3)\gamma_1 \sin^2\beta\left(\frac{4\sin\gamma_1 \sin\gamma_2}{3\gamma_1} + \sin\beta\right)$$

where

$\sin(\alpha+\beta) = \sin(18^\circ 50' + 22^\circ 50') = \sin 41^\circ 40' = 0.6648$

$\cos(\alpha-\beta) = \cos(18^\circ 50' - 22^\circ 50') = \cos 4^\circ = 0.9976$

$I_c = \frac{(93^4 - 92.5^4)}{4}[2 \times 0.8203 - 0.6648 \times 0.9976] + 2 \times 93 (93^3 - 92.5^3) \times 0.8203 \times 0.3871 \times \left(\frac{4 \times 0.7314 \times 0.4094}{3 \times 0.8203} + 0.3871\right) =$

$= \frac{1595787}{4}[1.6406 - 0.6632] + 186 \times 12904 \times 0.3175 \times (0.4867 + 0.3871) =$

$= 389{,}931 + 665{,}876 = 1{,}055{,}816$ in^4

d. Moment of Inertia of the Tensile Area
According to formula (5.122)

$$I_c = (r^4 - r_1^4)\left\{\frac{1}{8}[2(90-\beta) - \sin 2\beta + 4\cos^3\beta\sin\beta] + \frac{8}{9}\frac{\cos^6\beta}{2(90-\beta) - \sin 2\beta}\right\} - \frac{4}{3}r(r^3 - r_1^3)\cos^5\beta\sin\beta + \frac{r^2(r^2 - r_1^2)}{2}[2(90-\beta) - \sin 2\beta]\sin^2\beta$$

where

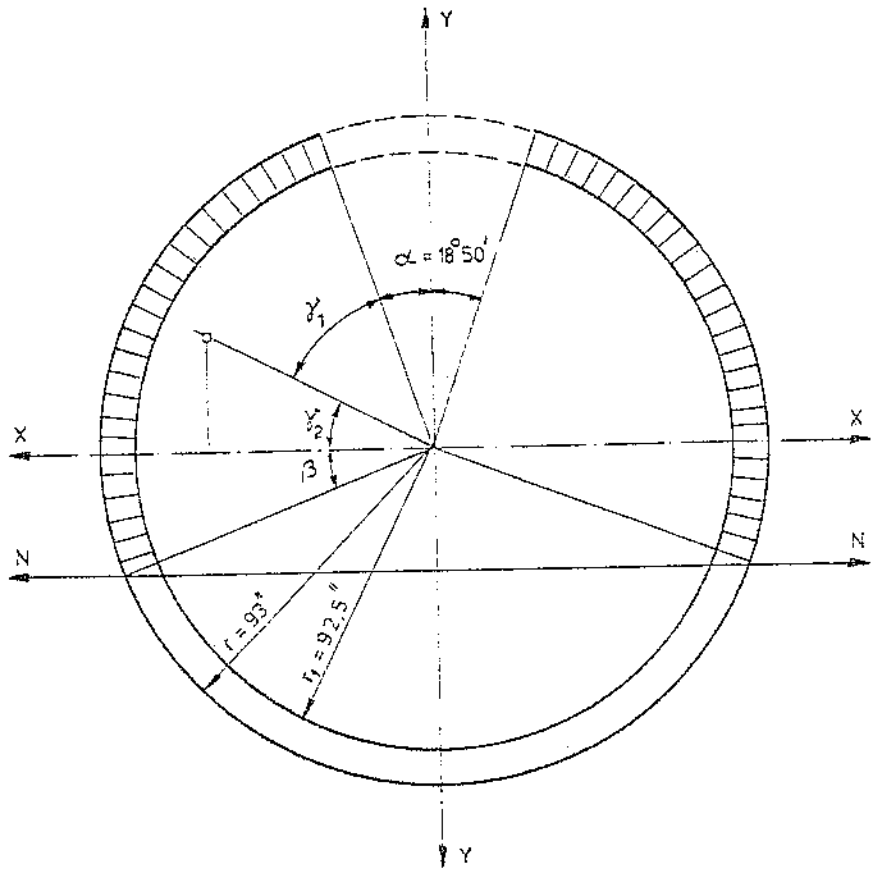

FIGURE 5.36 — Geometric data for statical moments of compressed and tensile areas.

$$\frac{2(90-\beta)}{57.296} = \frac{2(90 - 22^\circ 50')}{57.296} = \frac{134.333}{57.296} = 2.3445$$

$$\sin 2\beta = \sin 45^\circ 40' = 0.7153$$

$$\cos^3\beta = \cos^3 22^\circ 50' = 0.9216^3 = 0.7828$$

$$\sin\beta = \sin 22^\circ 50' = 0.3871$$

$$\cos^6\beta = \cos^6 22^\circ 50' = 0.9216^6 = 0.6127$$

$$\sin^2\beta = \sin^2 22^\circ 50 = 0.3871^2 = 0.1498$$

$$r(r^3 - r_1^3) = 93(93^3 - 92.5^3) = 93(804357 -$$

$$- 791453) = 93 \times 12904 = 1{,}200{,}072$$

$$r^2(r^2 - r_1^2) = 93^2(93^2 - 92.5^2) =$$

$$= 8649\ (8649 - 8556.25) =$$

$$= 8649 \times 92.75 = 802195$$

$$I_T = 1595787 \left\{ \frac{1}{8} \left[2.3445 - 0.7153 + 4 \times \right. \right.$$

$$\left. \left. \times 0.7828 \times 0.3871 \right] + \frac{8}{9} \frac{0.6127}{2.3445 - 0.7153} \right\} -$$

$$- \frac{4}{3} \times 1200072 \times 0.7828 \times 0.3871 +$$

$$+ \frac{802195}{2} \left[2.3445 - 0.7153 \right] 0.1498 =$$

$$= 1595787 \left\{ \frac{1}{8} \left[1.6292 + 1.2121 \right] + 0.3345 \right\} -$$

$$- 483{,}652 + 97890 = 1595787 \times 0.6895 -$$

$$- 386974 = 1{,}100{,}235 - 386974 =$$

$$= 713{,}261 \text{ in}^4$$

As previously discussed, the derivation of this equation is incorrect and leads to an incorrect It. With an assumed yc of 36 in, It should equal about 180,421 in^4

6. Part 6. Checking of the Value of Axial Load N. According to formula (5.82) the value of the coefficient ϕ is

$$\phi = \frac{M_w + Px_o}{I_c + I_T} = \frac{25{,}172{,}250 + 119{,}000 \times 36}{1{,}055{,}855 + 713{,}261} =$$

$$= \frac{29{,}456{,}250}{1{,}679{,}116} = 16.65 \text{ lb/in}^3$$

From formula (5.83) it follows

$N = \phi (S_c - S_T) = 16.65\ (10{,}616 - 4{,}015) =$

$= 16.65 \times 6{,}614 = 109{,}907$ lb

$109{,}907 < 114{,}768$

Difference is 4.42%

This means guess of 36 in was a little off. Our example calculated Yc = 26.82 in, and that led to difference of 0

7. Part 7. Determination of Stresses

The average compressive stress in the wall is estimated after formula (5.88)

$$f_{av} = \frac{\phi S_c}{t} \times \frac{180}{\pi(r+r_1)\ (90-\alpha+\beta)}$$

where

$$90 - \alpha + \beta = 90 - 18^\circ 50' + 22^\circ 50' = 94^\circ$$

$$f_{av} = \frac{16.65 \times 10.616}{0.5} \times \frac{180}{3.14\ (93 + 92.50)\ 94} =$$

$$= 35{,}3513 \times \frac{180}{54{,}752} = 1162 \text{ psi}$$

The maximum stress at the middle of the wall after formula (5.91)

$$f_{max} = \frac{\phi}{2} \left[2x_c + (r + r_1) \cos\alpha\right]$$

where $x_c = 36$ in

$$\cos\alpha = \cos 18^\circ 50' = 0.9465$$

$$f_{max} = \frac{16.65}{2} \left[2 \times 36 + (93 + 92.5) \times 0.9465\right] =$$

$$= \frac{16.65}{2} \times 248 = 2{,}065 \text{ psi}$$

8. Part 8. Determination of Stresses by the Experimental Method

Nondimensional geometric parameter, $\bar{r}$ according to formula (5.125) is

$$\bar{r} = \frac{a + b}{4\sqrt{Rt}}$$

For

a = 5 ft. - 60 in.

b = 8 ft. = 96 in.

R = 93 in.

t = ½ in.

$$\bar{r} = \frac{60 + 96}{4\sqrt{93 \times 0.5}} = \frac{39}{\sqrt{46.5}} = 5.72$$

From Figure 5.23. for $\bar{r} = 5.72$, we find:

$$\frac{P}{P_{cl}} = 0.22$$

MecaStack based upon lower bound curve and got 0.186

$$\frac{P}{P_{cl}} = 0.6\ E \left(\frac{t^2}{R}\right)$$

Doesn't say what to do with the P calculated. Refer to our article where we explain what MecaStack does with P/Pcl.

Therefore,

$$P = 0.22 \times 0.6\ E \left(\frac{t^2}{R}\right) = 0.132\ E \left(\frac{t^2}{R}\right)$$

or

$$P = 0.132 \times 30 \times 10^6 \times \frac{0.5^2}{93} = 10{,}645 \text{ lb/in}$$

9. Part 9 Design of Stiffeners at Breech Opening

a. The required cross-sectional area of the single vertical stiffener after formula (5.128)

$$A_s = \frac{tR^2 \sin\alpha}{d}$$

Assume $d = 93\cos\alpha - 5 = 93''$

$\sin\alpha = \sin 18^\circ 50' = 0.3228$

$$A_s = \frac{0.5 \times 93^2 \times 0.3228}{93.00} = 15.00 \text{ in}^2$$

b. Moment of inertia of removed part about a stack center line after formula (5.138) is

$$I_{rem} = R^3 \left(\alpha + \frac{\sin 2\alpha}{2}\right) t$$

where $\alpha = 18^\circ 50'$, $\alpha(\text{rad}) = \frac{18.83}{57.296} = 0.3286$

$\sin 2\alpha = \sin 37^\circ 40' = 0.6111$

$$I_{rem} = 93^3 \left(0.3286 + \frac{0.6111}{2}\right) \times 0.5 =$$

$$= 804357 \times 0.6341 \times 0.5 =$$

$255{,}021$ in⁴

$$2I_{stiff} \geq I_{rem}$$

Therefore, required

$$I_{stiff} = \frac{I_{rem}}{2} = \frac{255021}{2} = 127{,}510 \text{ in}^4$$

Try 10WF54, $A = 15.9$ in²

$$I_x = 306.0 + 15.9 \times 93^2 = 306.0 + 137{,}578 =$$

$= 137{,}884$ in⁴

MecaStack took Stiffener area and also local I for member, so our value calculated was higher.

c. The axial compressive stress in each stiffener under the weight of the wall above the breech opening according to formula (5.130) is

$$f_G = \frac{C}{A_s} \times \frac{\alpha}{360} = \frac{114{,}768}{15.9} \times \frac{18.88}{360} = 378 \text{ psi}$$

d. The axial compressive stress in each stiffener due to the wind load moment, after formula (5.134)

$$f_w = \frac{M_w d\alpha}{22.5\ t\ D_m^2\ \sin\alpha}$$

$$f_w = \frac{25172250 \times 93 \times 18.83}{22.5 \times 0.5 \times 185.5^2 \times 0.3228} = 1902 \text{ psi}$$

e. The axial compressive stress due to the eccentricity of stiffener, after formula (5.136)

$$f_e = \frac{(G + P_w)e}{S_{stiff}}$$

where

$$G = 114{,}768 \times \frac{18.83}{360} = 6003 \text{ lbs}$$

$$P_w = \frac{M_w a}{90 D_m} = \frac{25172250 \times 18.83}{90 \times 185.5} = 28391 \text{ lbs}$$

$$e = 5 \text{ in.}$$

$$S_{stiff} = 60.5 \text{ in}^3$$

$$f_e = \frac{(6003 + 28391) \times 5}{60.5} = 2842 \text{ psi}$$

f. Total axial stress in vertical stiffener is sum of .

$$f_{tot} = f_G + f_w + f_e$$

$$f_{tot} = 378 + 1902 + 2842 = 5122 \text{ psi}$$

MecaStack uses AISC 360-16 which uses Forces rather than stress, so we calcualted total force rather than stress.

g. Buckling Stability of Vertical Stiffeners

Vertical stiffeners under action of axial load and bending moments due to the eccentricity of axial loads at both ends, may be considered as beam-columns. The maximum buckling stress is estimated using formula (5.148)

$$\sigma_{max} = \frac{P}{A} + \frac{M_o c}{I} \sec\frac{h}{2}\sqrt{\frac{P}{EI}}$$

where P is a part of axial load acting on vertical stiffener

$$P = 114{,}768 \times \frac{18.83}{360} = 6003 \text{ lbs}$$

Section properties for stiffener cross-section

A = 15.9 in^2

I = 306.0 in^4

S = 60.5 in^3

Bending moment acting on stiffener due to the wind

$$M_w = f_w S = 1902 \times 60.5 = 115{,}071 \text{ lb in}$$

Bending moment acting on stiffener due to the eccentricity of axial load

$$M_e = 114{,}768 \times \frac{18.83}{360} \times 5 = 30{,}015 \text{ lb in}$$

Total moment

$$M_o = M_w + M_c = 115{,}071 + 30{,}015 =$$

$$= 145{,}086 \text{ lb in}$$

$$\sigma = \frac{6003}{15.90} + \frac{145{,}086 \times 5}{306.0}$$

$$\sec\frac{96}{2}\sqrt{\frac{6224}{30 \times 10^4 \times 306.0}} =$$

$$= 378 + 2370 \sec 0.0395 =$$

$$= 378 + 2370 \sec 2^\circ 16' =$$

$$= 378 + 2370 \times 1.00078 = 2751 \text{ psi}$$

MecaStack uses AISC 360-16 for this member check.

h. Ring Girder

The total distributed load using formula (5.152)

$$w = \frac{G}{2\pi R} + \frac{M_w}{\pi R^2}$$

$$w = \frac{114{,}768}{2 \times 3.14 \times 92.75} + \frac{25172250}{3.14 \times 92.75^2} =$$

$$= 197 + 932 = 1{,}129 \text{ psi}$$

The bending moment in the girder

$$M = \frac{w\ell^2}{12} = \frac{1129 \times 60^2}{12} = 338{,}700 \text{ lb in}$$

Assuming $\sigma_{all} = 20{,}000$ psi

Required SM = $\frac{338700}{20000} = 16.94$ in^3

Use 10 x 5-3/4 21#

SM = 21.5 in^3 > 16.94 in^3

MecaStack doesn't follow this method exactly, since it is very conservative. Please refer to article for more explanation on our approach.

NUMERICAL EXAMPLE NO. 2
Rigorous Analysis. Application of Finite Element Method

1. INTRODUCTION

The purpose of this investigation is to study the stress distribution and stress concentrations around the breech opening for the individual and combined effects of dead and wind loads. The magnitude and the distribution of

stresses in the vicinity of the opening will determine whether it should be reinforced with additional steel or not. These concepts, along with the ones presented in Section 5.8, have been applied to the stress-analysis of a stack-opening as presented in the following pages.

2. DESCRIPTION OF STACK

The stack analyzed in this example, shown in Figure 5.37, has the following characteristic parameters:

Base diameter = 30.0 ft.; Top diameter = 15.0 ft.

Height = 500 ft.; Shell-plate thickness = 1.25 in.

The Young's modulus for the stack material is 29,000 ksi and its yield strength is 40 ksi. The breech, with dimensions 15.0 ft. × 10.0 ft. is located 8 ft. above the ground level.

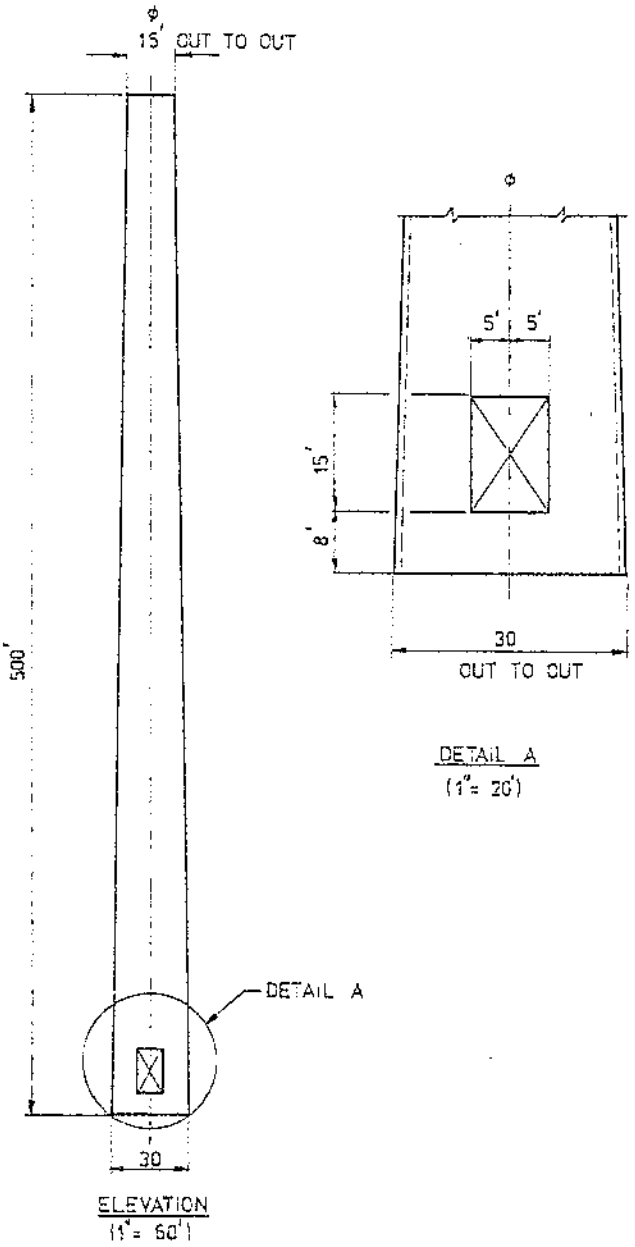

FIGURE 5.37 — Stack and breech dimensions.

3. DESCRIPTION OF FINITE ELEMENT MODELS

In order to study the stress distribution around the breech, two different finite-element-models were related. The first one (or Model I) was 50 ft. high from the base of the stack, while the second one (or Model II) was 200 ft. For a perspective view of Model II, see Figure 5.38 shown on this Figure are also the two major directions, along which the lateral wind has been assumed to act for stress-analysis purposes.

Having reviewed the computer output of Models I and II separately for identical loading conditions, it was concluded that results corresponding to the analysis of Model II should be presented in this report, since its discretization scheme had a much larger number of finite elements as compared to Model I and consequently could predict better results in the vicinity of the stack-opening. In addition, computer results also showed (for Model II analysis) that wind blowing from East to West produced greater stresses around the opening as contrasted to the wind from North to South. Therefore, these values were selected for all stress-calculations in the subsequent pages. Figures 5.39 and 5.40 represent the discretization scheme to the left and right of the opening, respectively, showing its element and node numbers. All element nodes were fed into the computer program in cylindrical coordinates.

Figures 5.41 to 5.46 show the plan view of the discretization scheme at elevations 0.0 ft., 50.0 ft., 80.0 ft., 120.0 ft., 160.0 ft., and 200.0 ft. The node numbers of elements are shown around the outer periphery of the diagram, while an angle subtended at the center of the circle by two adjacent nodes is indicated by an angle-figure shown between the two radii joining the nodes with the center. The change in the stack-radius from 179.375 in., Figure 5.41 to 143.375 in., Figure 5.46 is indicative of the vertical taper that the stack-geometry has a part of its configuration.

4. LATERAL WIND LOAD ON STACK

The lateral wind load on the stack has been calculated according to the National Building Code of Canada. The general equation for the lateral wind load, according to this code, on an exposed surface is as follows:

$$p = q \cdot C_e \cdot C_g \cdot C_p \cdot C_n$$

where

- q = the uniform lateral wind pressure in lbs/ft²;
- C_e = the exposure factor that varies according to the height of the structure;
- C_g = the gust factor;
- C_p = shape factor; and
- C_n = the additional shape factor for chimneys.

Typical values of the above factors were used as shown below

- q = 9.2 lbs/ft (For Montreal Area);
- C_e = varies from 1.0 for a height of 40 ft. to 2.0 for a height of 1200 ft.
- C_g = 2.0; C_p = 1.6 and C_n = 0.7

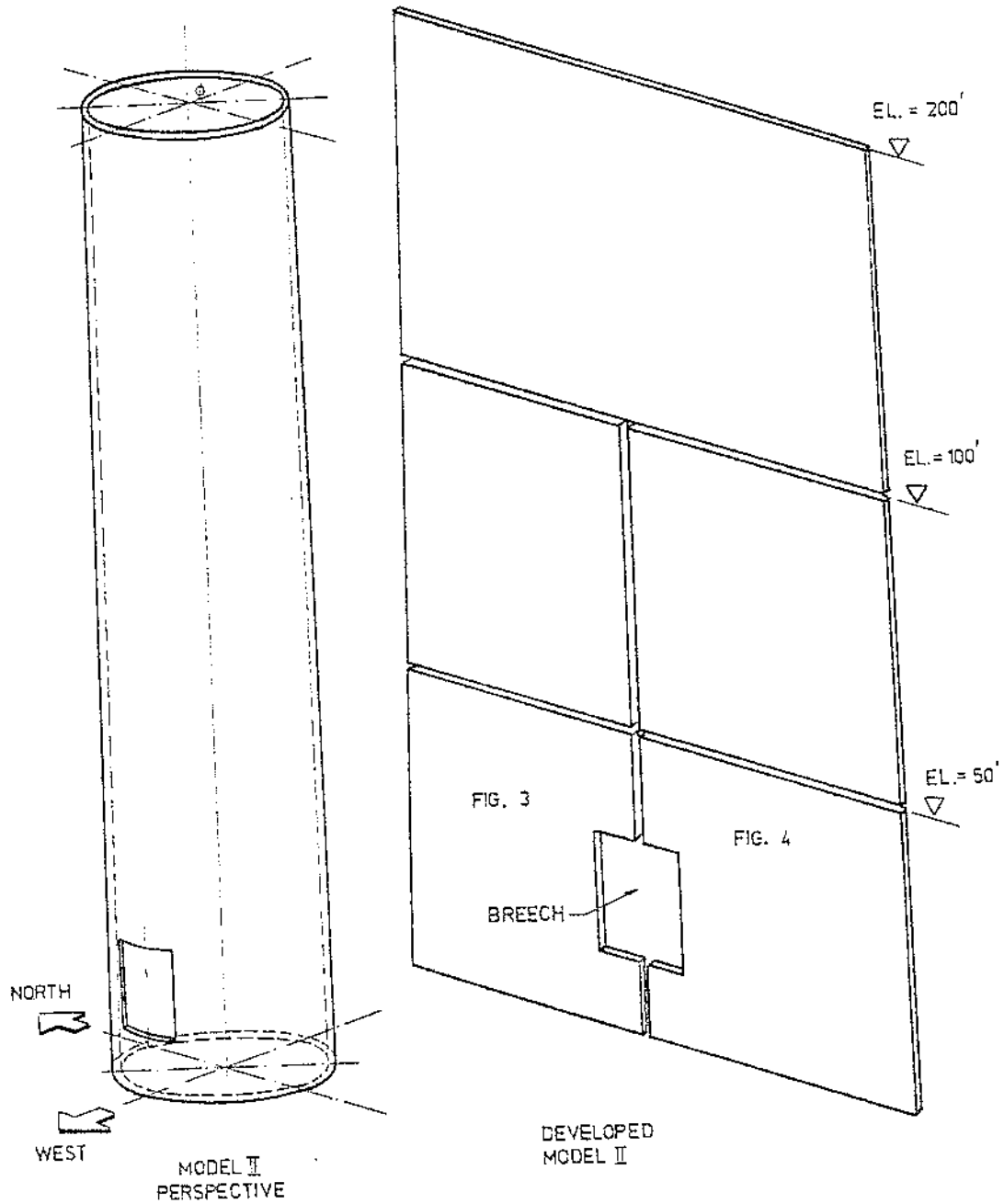

FIGURE 5.38 — Perspective of stack — Model II.

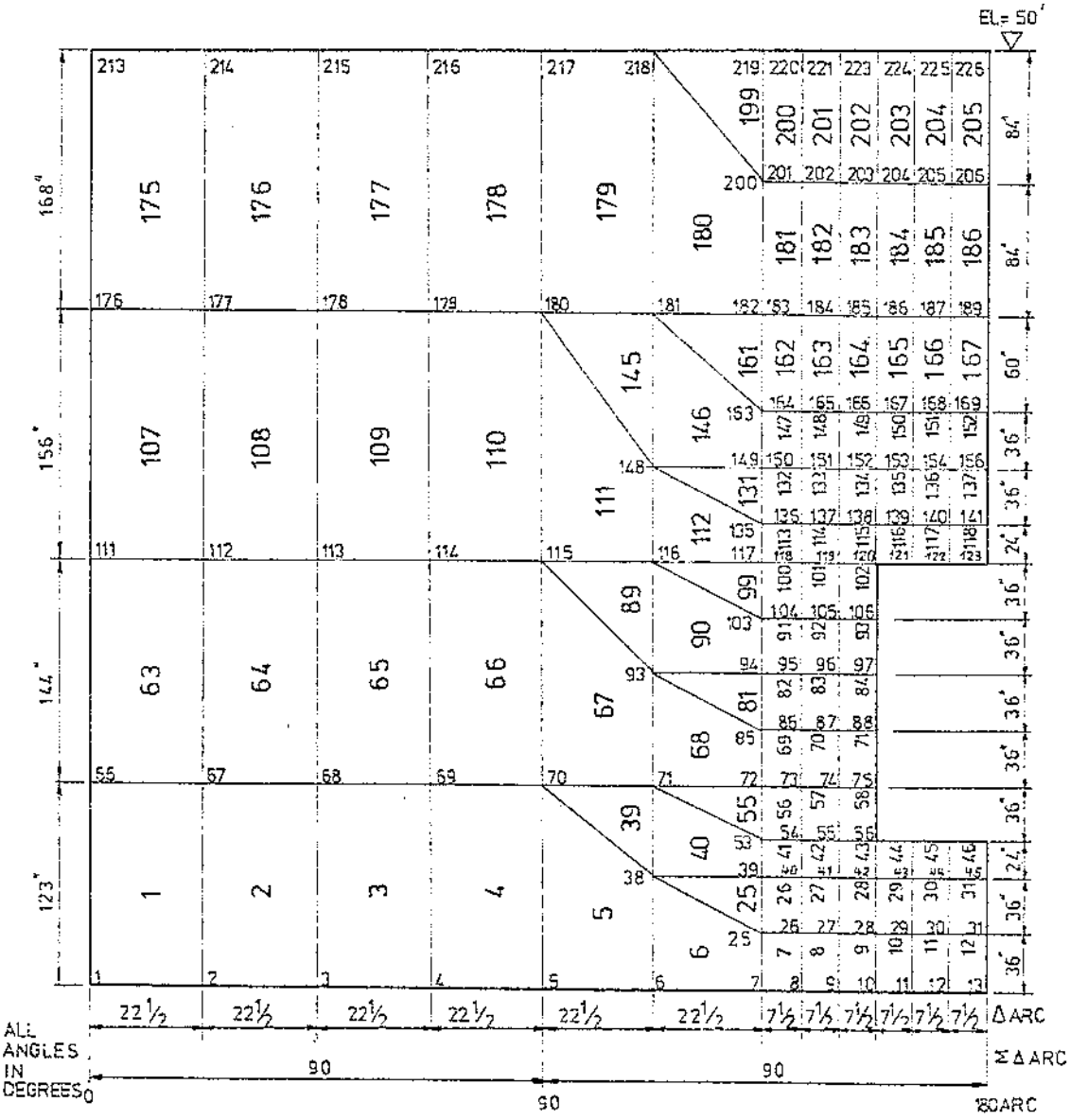

NOTE: The discretization scheme presented on Figure 5.39 is a developed view of the left half (with respect to the opening) of the truncated cone between stack elevations 0.0 and 50.0. The regular-shaped elements *i.e.* rectangles and triangles, and shown, are in fact distorted with vertical lines slightly inclining to the right and the horizontal ones with some curvature.

FIGURE 5.39 — Discretization scheme around opening.

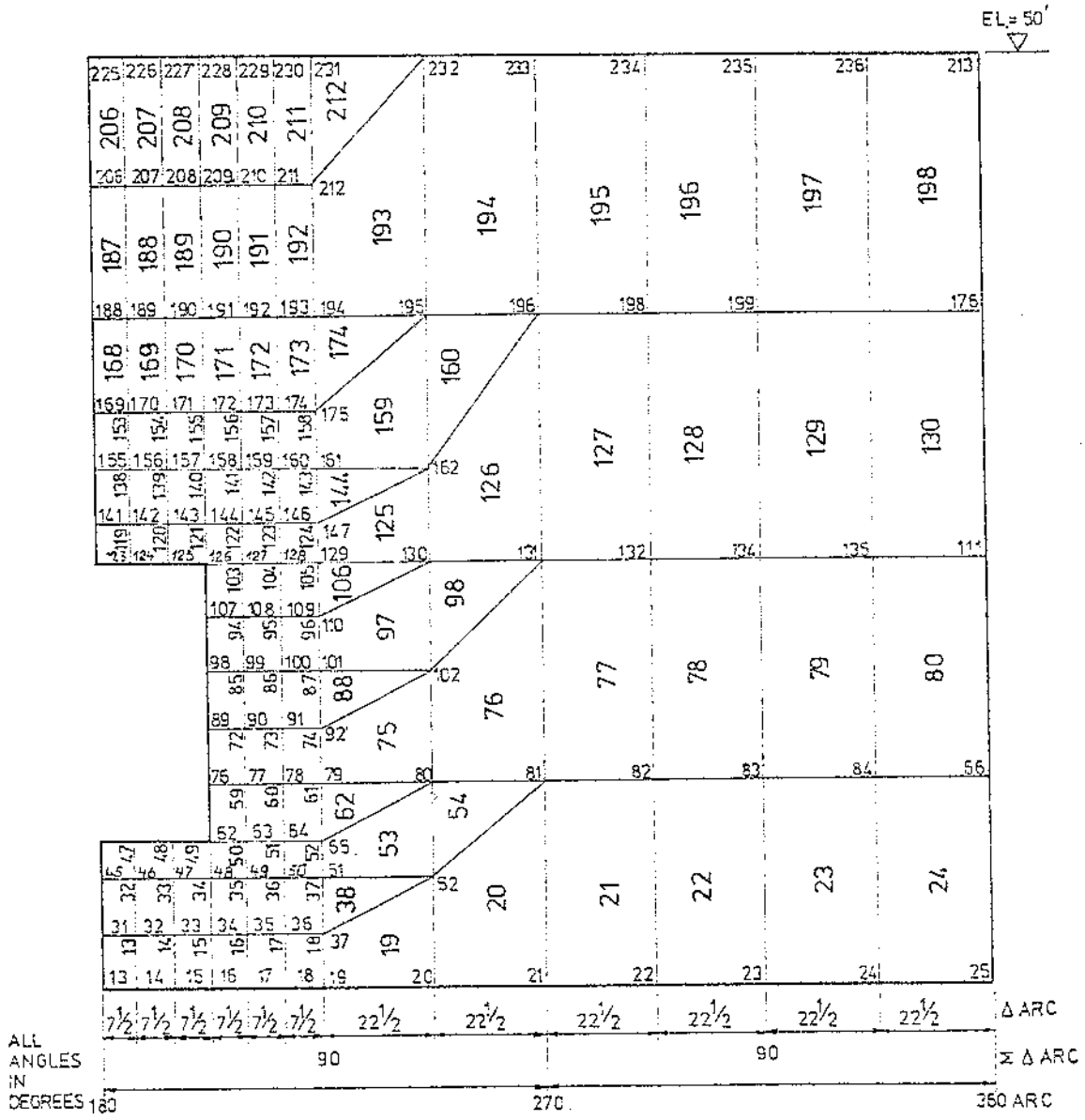

NOTE: The discretization scheme presented on Figure 5.40 is a developed view of the right half (with respect to the opening) of the truncated cone between stack elevations 0.0 and 50.0. The regular shaped elements *i.e.* rectangles and triangles, as shown, are in fact distored with vertical lines slightly inclining to the left and the horizontal ones with some curvature.

FIGURE 5.40 — Discretization scheme around opening.

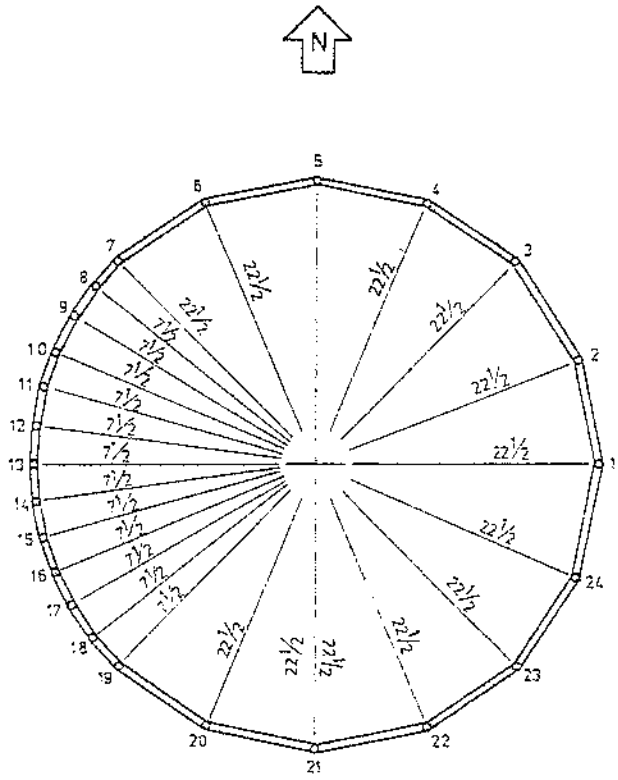

FIGURE 5.41 — Plan cross-section at El. = 0.0' cross-sectional radius = 179.375".

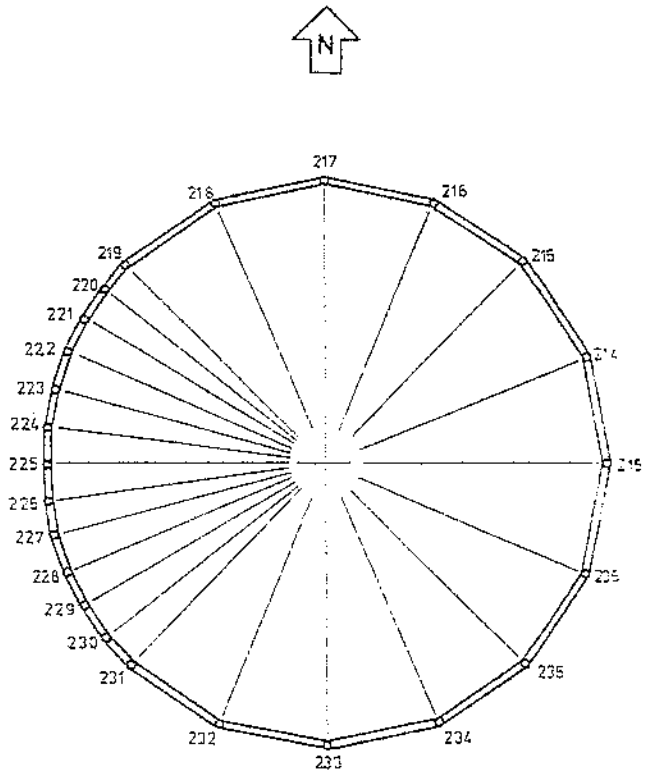

FIGURE 5.42 — Plan cross-section at El. = 50' cross-sectional radius = 170.375".

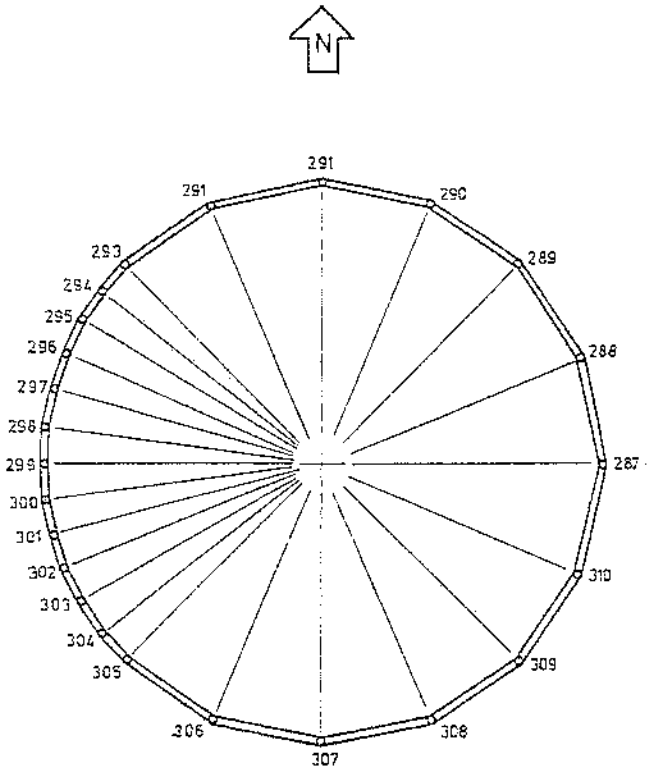

FIGURE 5.43 — Plan cross-section at El. = 80' cross-sectional radius = 164.975".

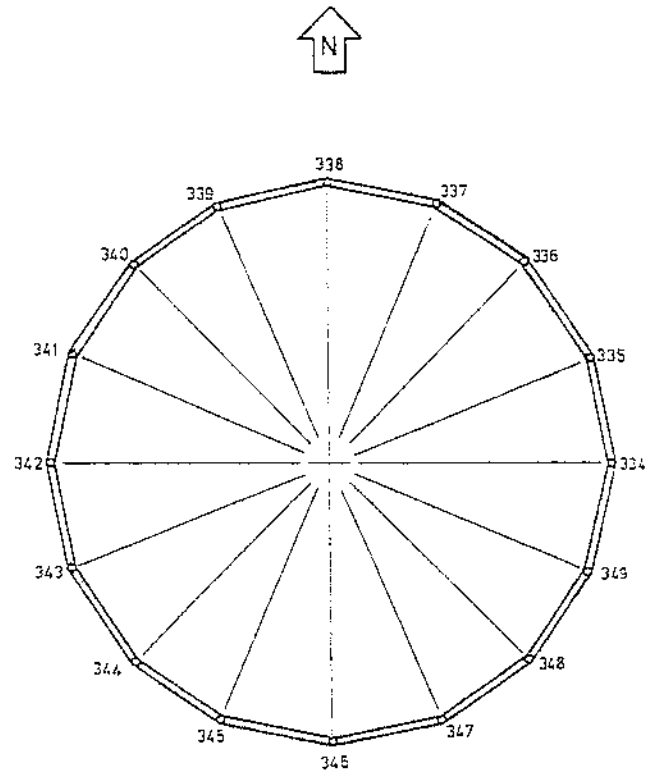

FIGURE 5.44 — Plan cross-section at El. = 180' cross-sectional radius = 157.775".

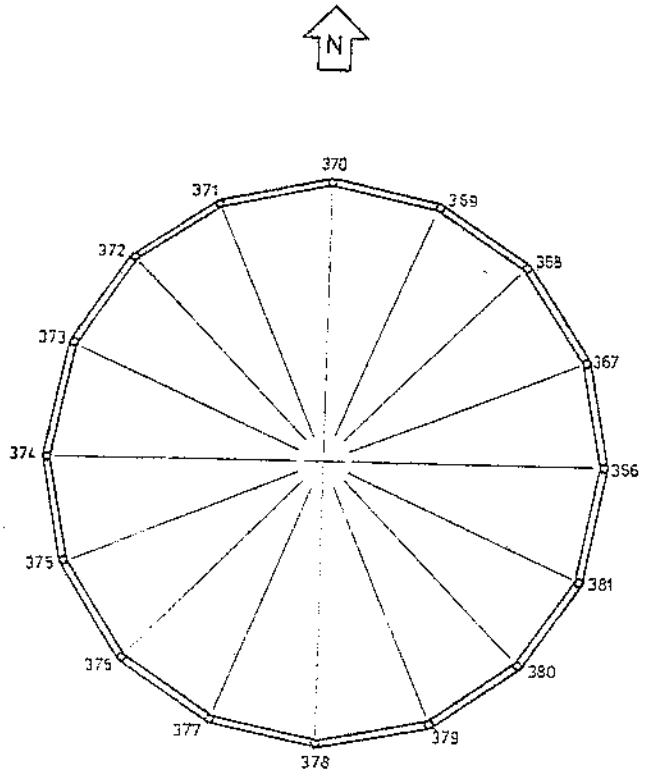

FIGURE 5.45 — Plan cross-section at El. = 160' cross-sectional radius = 150.575".

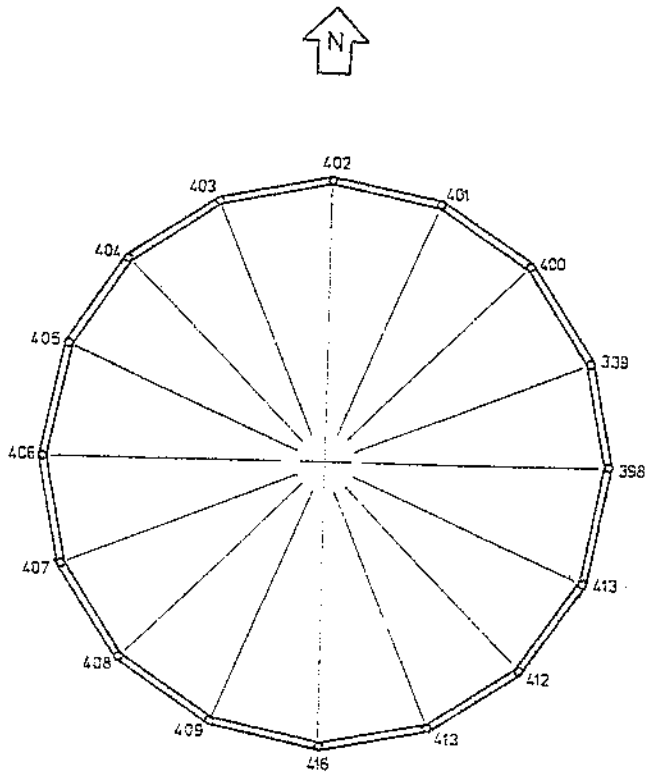

FIGURE 5.46 — Plan cross-section at El. = 200' cross-sectional radius = 143.375".

The diagrams for the lateral load appear on Figs. 5.47 and 5.48, for Models I and II respectively, where the wind load appears as a stepped function of the stack-height.

5. TRANSMISSION OF APPLIED FORCES ONTO STACK-MODEL-II

The forces acting on stack-model II are:

(i) Self-weight of the model (height — 200 ft.);

(ii) Dead load of the stack on top of the model acting vertically down; and

(iii) Lateral wind acting on the entire stack.

Figure 5.49 is a graphic display of the application of vertical line loads acting on the top edge of stack-model II due to lateral wind and self-weight of the stack. Moreover, Figure 5.50 shows how the transverse shear due to wind load can be applied to the same model by transforming it into equivalent tangential shear first. Such a conversion has been found very advantageous in ANSYS computer program and leads to substantial savings in computer time used and the cost incurred.

6. THEORETICAL ANALYSIS

The stress analysis of the area adjoining the stack-opening has been performed using the finite element method of analysis for Model I and Model II. However, for reasons given in Section 3 of Example No. 2, only results corresponding to Model II have been used in the following pages. Triangular and rectangular finite elements were chosen for the discretization scheme. ANSYS computer program was used for the stress analysis with loading conditions as dead load, wind load and their combination. The output gave results in terms of bending and membrane stresses, bending and torsional moments and axial loads as well as displacements of elements and nodes. (For detailed results, refer to the computer output).

7. TABULATION OF COMPUTER RESULTS

In order to design the reinforcement around the opening, the most critical combination of external loads on the stack was selected i.e., dead load + lateral E. to W. wind load, Figure 5.48. Moments and axial forces corresponding to this loading condition have been tabulated in Tables 5.8 to 5.11 for elements in the immediate vicinity of the opening, Figures 5.39 and 5.40.

8. DESIGN OF VERTICAL STIFFENERS

It will be assumed that the stiffeners will act integrally with the stack and as such a certain length of the stack plate will have a significant stiffening effect on the stiffeners. In order to determine this length, reference is made to the AISC Specifications for stiffeners of plate girder webs. Notwithstanding the slight disparity between the behavior of a steel stack plate and a plate girder web, we believe we can make use of the following specification with some reservation [5.75].

MODEL I WIND LOADS

The wind moments and shears for Model I were determined tabularly, Table 5.7 in accordance with Fig. 5.47.

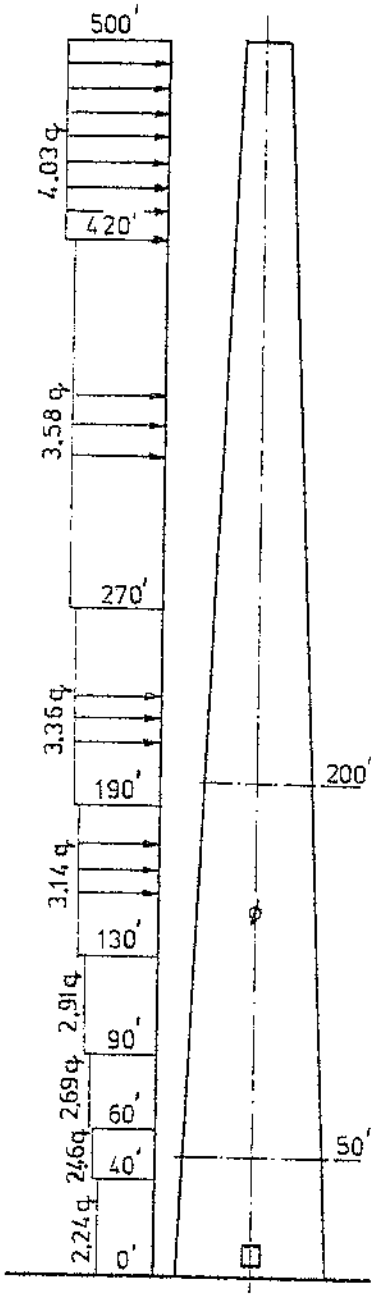

FIGURE 5.47 — Elevation of wind intensity against stack wrt to stack El. in gpsf.

TABLE 5.7

STACK ELEV FT	ELEV DIFF FT	AVG DIAM FT	AVG AREA FT^2	LAT. WIND qPSF	LAT. SHEAR q#	MOM ARM ABT BASE FT	MOMENT ABT BASE q#-FT	MOM ARM ABT. EL=50' FT	MOMENT ABT EL=50' q#-FT
0									
	40	29.4	1176	2.24	2634	20	52680	0	0
40					701				
	20	28.5	570	2.46	----	50	70100	5	3500
60					701				
	30	27.8	833	2.69	2239	75	167925	25	55975
90									
	40	26.7	1068	2.91	3108	110	341880	60	186480
130									
	60	25.2	1512	3.14	4748	160	759680	110	522280
190									
	80	23.1	1848	3.36	6209	230	1428070	180	1117620
270									
	150	19.7	2948	3.58	10552	345	3640440	295	3112840
420									
	80	15.2	1296	4.03	5223	460	2402580	410	2141430
500									
TOTALS AT									
BASE					36115q		8863355 q		
EL. = 50'					32780q				7140125 q

TABLE 5.7 — Table of base and top of Model I lateral wind shears and overturning moments.

Note: The values shwon are for q = 1.0 PSF. For absolute values, they must be multiplied by chosen value of q. For Model I the analysis stresses due to the unit wind were multiplied by q = 9.2, the 1/100 wind for Montreal.

MODEL II LATERAL WIND

Wind forces for Model II, determined with respect to the wind distribution shown in Figure 5.48 and q = 9.2 psf, were as shown.

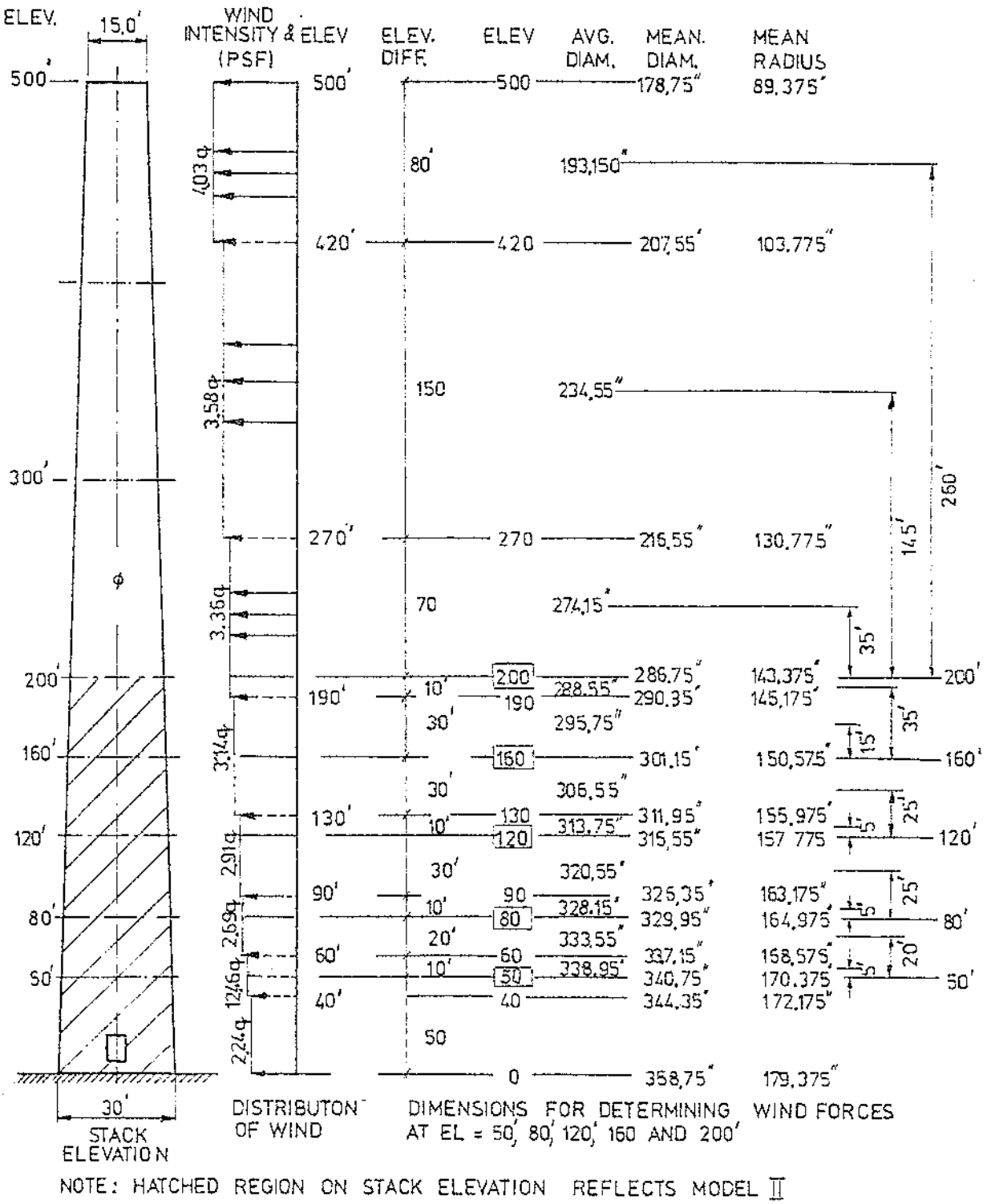

FIGURE 5.48 — Model II region and dimensions required to determine wind forces at node elevations shown.

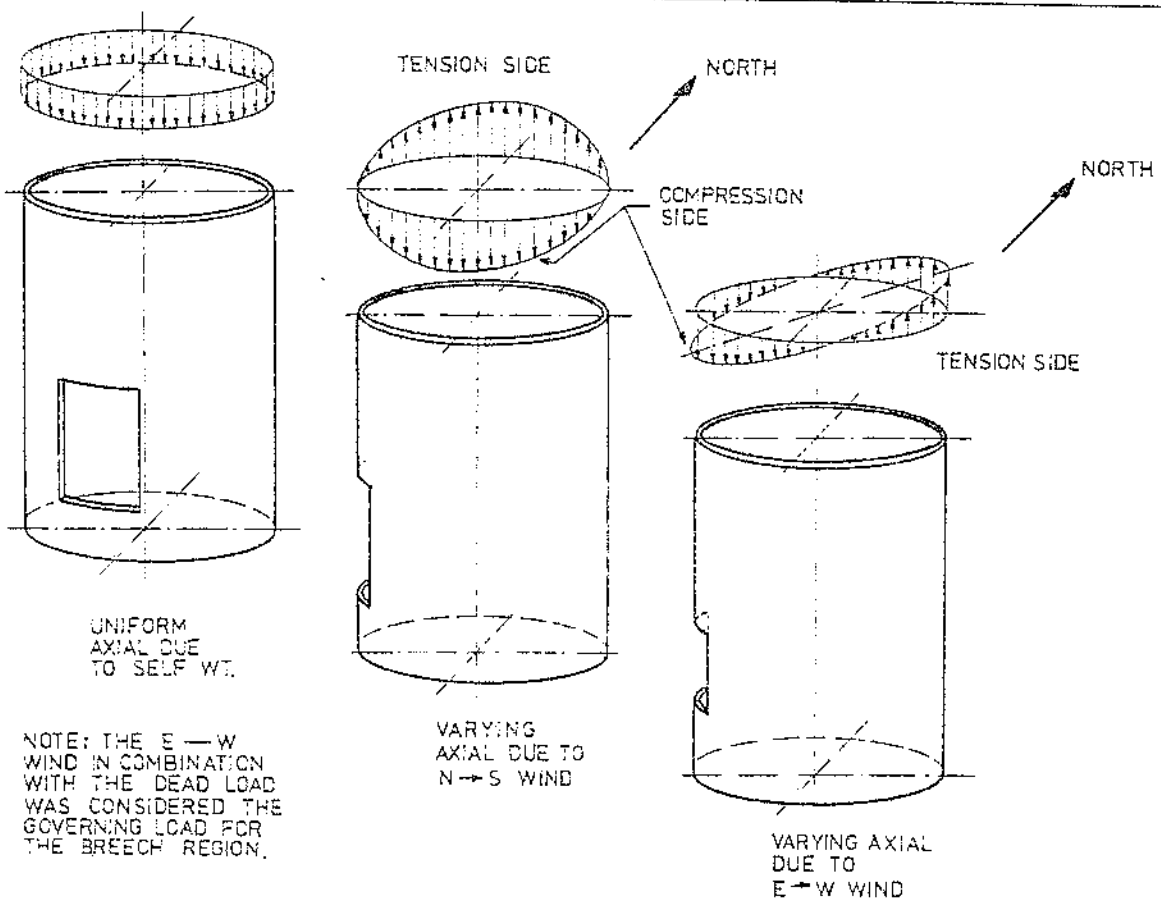

FIGURE 5.49 — Model II top edge vertical line loads due to lateral wind and self-weight dead load.

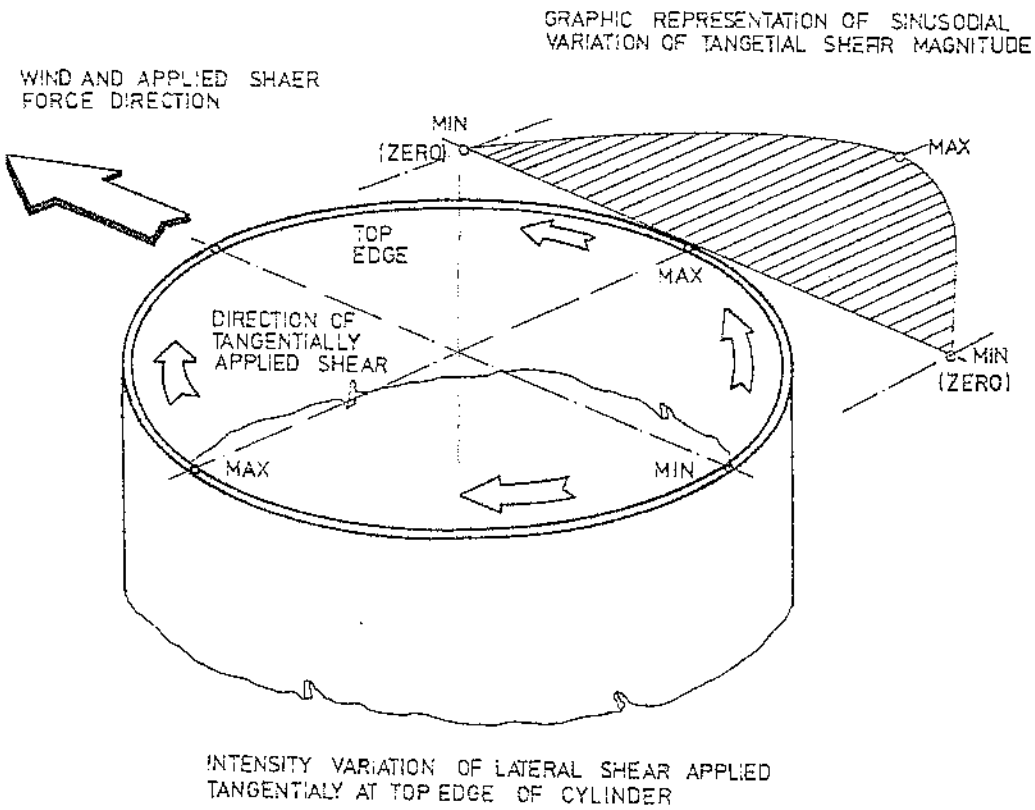

FIGURE 5.50 — Lateral shear along cylindrical plan cross-section.

TABLE 5.8 — Moments and Axial Forces in the Vertical Row of Elements.

(To the left of opening)

Note: Moments are in in-lbs/in whereas axial forces are in lbs/in.

El. No.	Mx	My	Nx	Ny
28	70	13	1	-4
43	244	-493	-14	-9
58	385	-119	-24	12
71	216	332	-21	-12
84	49	199	-12	0
93	339	694	-42	25
102	1221	653	-11	22
115	1450	27	28	-32
143	190	67	-23	5

Note: For an isometric plot of Moments M_x and M_y around opening, see Figures 5.51 and 5.52.

TABLE 5.9 — Moments and Axial Forces in the Vertical Row of Elements.

(To the right of opening)

Note: Moments are in in-lbs/in whereas axial forces are in lbs/in.

El. No.	Mx	My	Nx	Ny
35	70	13	-1	-4
50	244	-493	14	-9
59	385	-119	24	12
72	216	332	21	-12
85	49	199	12	0
94	339	694	42	25
103	1221	653	11	22
122	1450	27	-28	-32
141	698	-27	-8	-20

Note: For an isometric plot of moments M_x and M_y around opening, see Figures 5.51 and 5.52.

TABLE 5.10 — Moments and Axial Forces in the Horizontal Row of Elements.

(At the bottom of opening)

Note: Moments are in in-lbs/in whereas axial forces are in lbs/in.

El. No.	Mx	My	Nx	Ny
42	321	-169	-5	32
43	244	-493	-14	-9
44	-26	-75	-80	6
45	-505	7	19	-19
46	-158	2	20	4
47	-158	2	-20	4
48	-505	7	-19	-19
49	-26	-75	80	6
50	244	-493	14	-9
51	321	-169	5	32

Note: For an isometric plot of moments M_x and M_y around opening, see Figures 5.51 and 5.52.

TABLE 5.11 — Moments and Axial Forces in the Horizontal Row of Elements.

(At the top of opening)

Note: Moments are in in-lbs/in whereas axial forces are in lbs/in.

El. No.	Mx	My	Nx	Ny
114	774	265	55	-32
115	1450	27	28	-32
116	1565	146	-223	-21
117	-918	-7	-99	32
118	-1826	-242	-23	-9
119	-1826	-242	23	-9
120	-918	-7	99	32
121	1565	146	223	-21
122	1450	27	-28	-32
123	774	265	-55	-32

Note: For an isometric plot of moments M_x and M_y around opening, see Figures 5.51 and 5.52.

AISC Specification 1.10.5.1:

> Bearing stiffeners shall be placed in pairs at unframed ends on the webs of plate girders and where required at points of concentrated loads. They shall be designed as columns subject to the provisions of Section 1.5.1, assuming the column section to comprise the pair of stiffeners and centrally located strip of the web whose width is equal to not more than 25 times its thickness at interior stiffeners or *a width equal to not more than 12 times its thickness when the stiffeners are located at the end of the web.*

NOTE: Since the output of moments and forces is given in per inch of width, it will be assumed that the contributing width for the forces acting on vertical stiffeners would be 24 in. This is a matter of pure judgement. By scanning the computer output for the two consecutive rows of elements immediately around the opening, it is obvious that moments, shears and axial forces are significantly lower in the second row as compared to their counterparts in the first row (i.e. right next to the opening). Therefore, it is felt that the design of stiffeners should be based on the forces contributed by the entire width of the first row of element via 24 in.

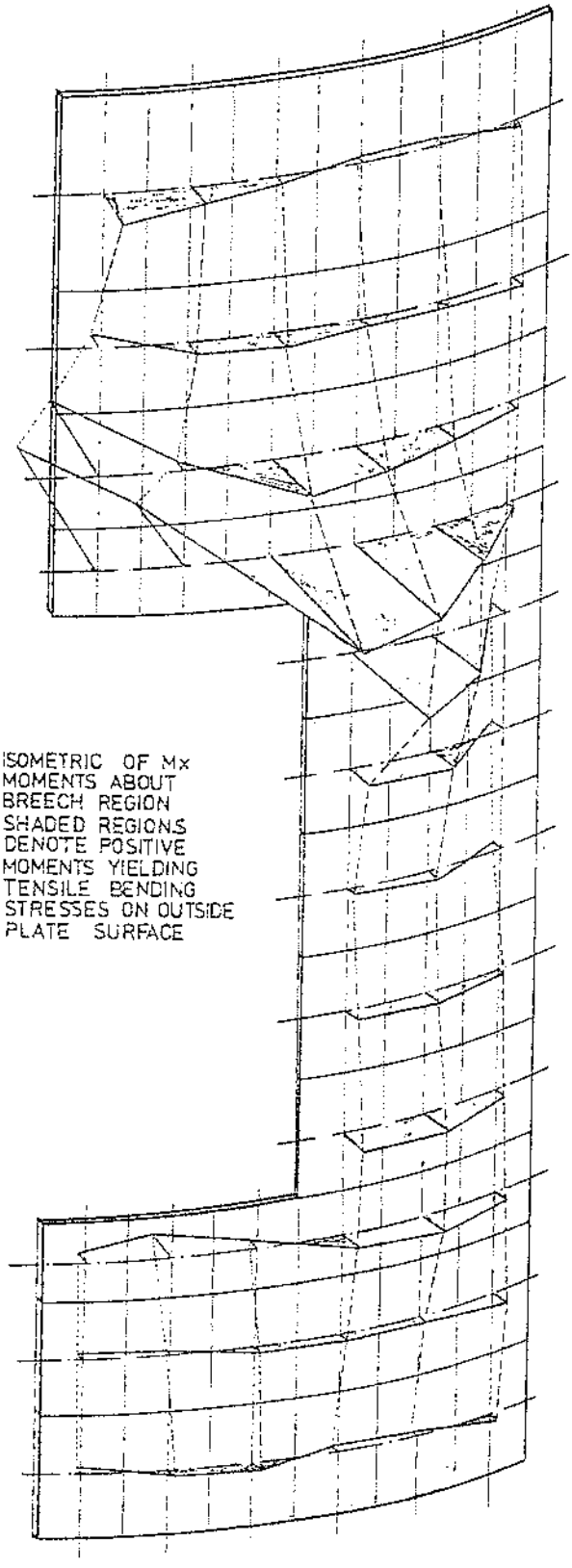

FIGURE 5.51 — Isometric plot of moment, Mx around opening.

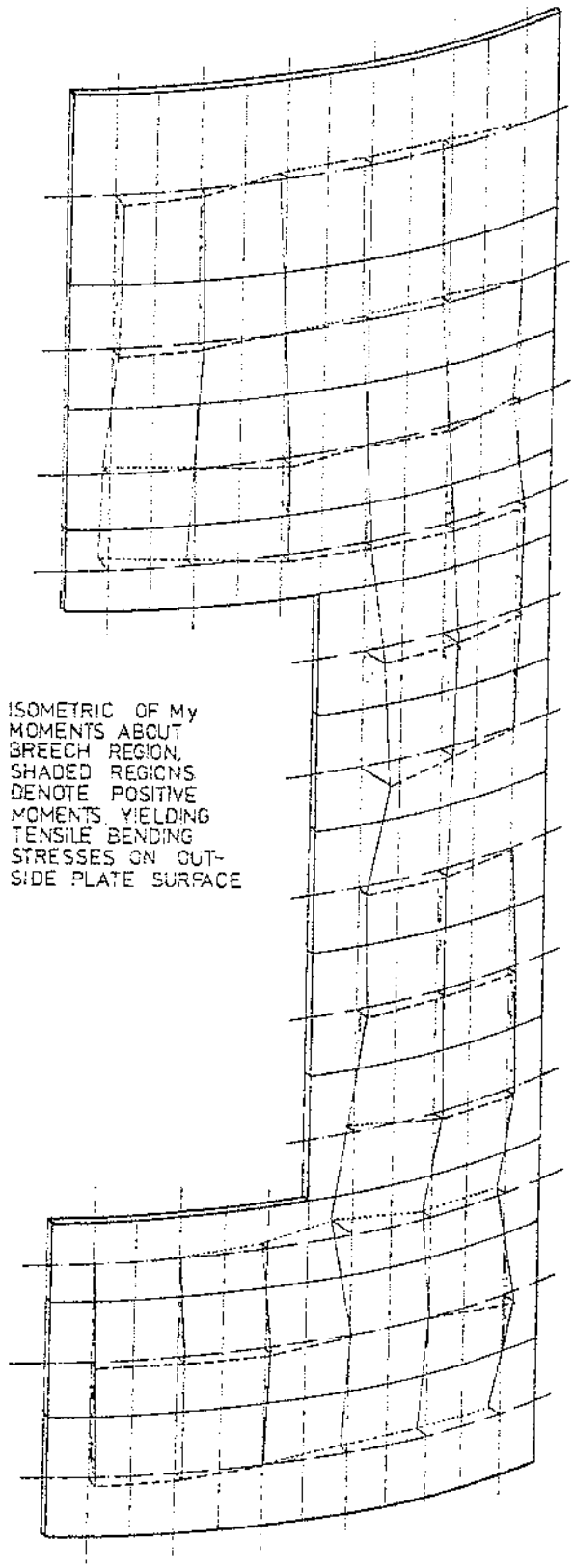

FIGURE 5.52 — Isometric plot of moment, My around opening.

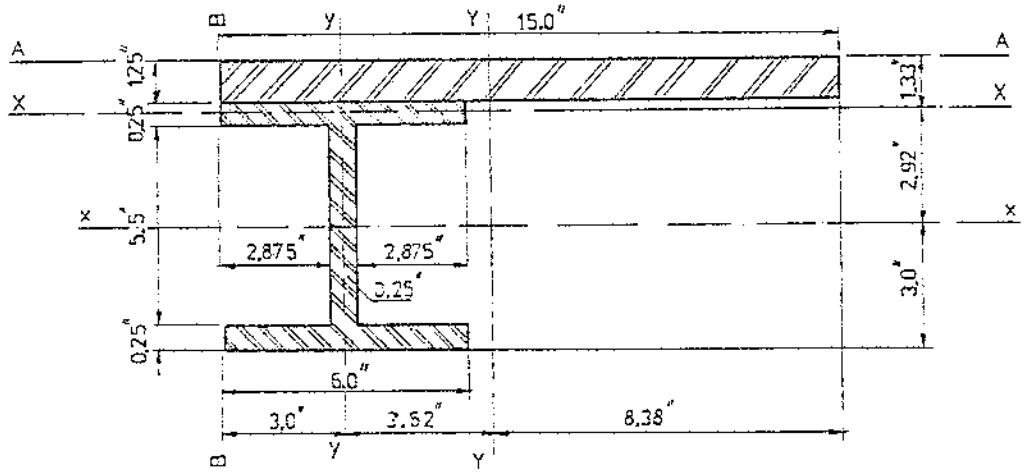

FIGURE 5-53 — Composite vertical stiffener and stack plate section.

Select a WF 6 shape @ 15.5 with the following properties:

A = 4.56 in²
Ix = 30.1 in⁴
Sx = 10.0 in³
rx = 2.57 in

and

Iy = 9.67 in⁴
Sy = 2.23 in³
ry = 1.46 in

Flange thickness t = ½ in and web thickness = ½ in

Stack plate thickness = 1.25 in

Stiffening width of stack plate = 12 × 1.25 = 15 in.

8.1 Determination of Neutral Axes of Composite Section

Taking moments about axis A-A we have:
Σ Area moments about axis

$$A\text{-}A = 4.56\,(3 + 1.25) + 15 \times 1.25 \times \frac{1.25}{2} = 19.38 + 11.72 =$$

$$= 31.10 \text{ in}^3$$

Taking moments about axis B-B we have
Σ Area moments about axis

$$B\text{-}B = 4.56 \times 3.0 + 15 \times 1.25 \times \frac{15}{2} = 13.68 + 140.63 =$$

$$= 154.31 \text{ in}^3$$

Total cross-sectional area = 4.56 + 15 × 1.25 = 23.31 in²

The neutral axis x-x is located at 31.10 ÷ 23.31 in from axis A-A = 1.33 in, and;

The neutral axis Y-Y is located at 154.31 ÷ 23.31 in from axis B-B = 6.62 in.

8.2 Determination of I_{xx} and I_{yy}

$$I_{xx} = 30.1 + 4.56\,(2.92)^2 + \frac{15 \times 1.25^3}{12} +$$

$$+ (15 \times 1.25) \times (1.33 - .63)^2 =$$

$$= 30.1 + 38.88 + 2.44 + 9.19 = 80.61 \text{ in}^4$$

$$r_{xx} = \left(\frac{80.61}{23.31}\right)^{\frac{1}{2}} = 1.86 \text{ in.}$$

$$S_{xx} = \frac{80.61}{1.32} = 60.61 \text{ in}^3$$

$$I_{yy} = 9.67 + 4.56\,(3.62)^2 + \frac{1.25(15)^3}{12} +$$

$$+ (15 \times 1.25) \times (8.38 - 7.5)^2 = 9.67 +$$

$$+ 59.76 + 351.56 + 14.52 = 435.51 \text{ in}^4$$

$$r_{yy} = \left(\frac{435.51}{23.31}\right)^{\frac{1}{2}} = 4.32 \text{ in.}\quad S_{yy} = \frac{435.51}{6.62} =$$

$$65.79 \text{ in}^3$$

The opening is 10 ft. wide and 15 ft. high. It is assumed that the stiffeners will be welded to the stack plate around the opening.

Assumed length = 18.0 ft. End conditions assumed as simply-supported. ∴ K = From Tables 5.8 and 5.9.

Max. M_y = 694 × 24 = 16,656 in lbs.

Max. N_y = 25 × 24 = 600 lbs.

$$\frac{K\lambda}{r_{xx}} = \frac{18 \times 12}{1.86} = 116 \text{ ; and}$$

$$\frac{K\lambda}{r_{yy}} = \frac{18 \times 12}{4.32} = 50$$

$$C_c = \left(\frac{2\pi^2 E}{F_y}\right)^{\frac{1}{2}} = \left(\frac{2 \times 3.14^2 \times 29{,}000}{40}\right)^{\frac{1}{2}} = 120$$

Since $\frac{K\ell}{r_{xx}} < C_c$

$$F.S. = \frac{5}{3} + \frac{3\left(\frac{K\ell}{r_{xx}}\right)}{8C_c} - \frac{\left(\frac{K\ell}{r_{xx}}\right)^3}{8C_c^3} =$$

$$= \frac{5}{3} + \frac{3 \times 116}{8 \times 120} - \frac{116^3}{8 \times 120^3} =$$

$$= 1.67 + 0.36 - 0.11 = 1.92$$

$$F_a = \frac{\left[1 - \frac{\left(\frac{K\ell}{r_{xx}}\right)^2}{2C_c^2}\right] F_y}{F.S.} = \frac{\left[1 - \frac{116^2}{2 \times 120^2}\right] 40}{1.92} =$$

$$= 11.04 \text{ ksi}$$

According to AISC Specification 1.5.1.4.4.

$F_b = 0.6\ F_y = 0.6 \times 40 = 24$ ksi

$f_a = \frac{600}{23.31} = 25.74$ psi; and

$f_b = \frac{16,656}{60.61} = 274.81$ psi;

$\frac{f_a}{F_a} = \frac{25.74}{11040} = 0.0023$;

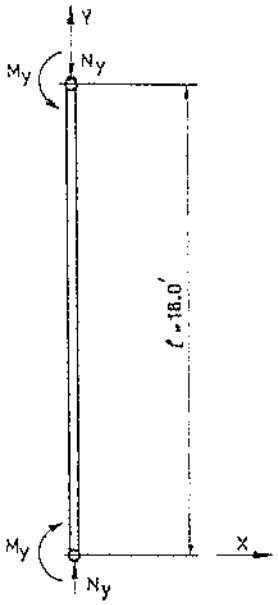

FIGURE 5.54 — Vertical Stiffener.

Since $\frac{f_a}{F_a} < 0.15$, use the criterion $\frac{f_a}{F_a} + \frac{f_b}{F_b} \leq 1.0$; hence

$$\frac{f_a}{F_a} + \frac{f_b}{F_b} = \frac{25.74}{11040} + \frac{274.81}{24,000} = 0.0023 + 0.01145$$

$$= 0.01375 \leq 1.0 \text{ Hence quite safe}$$

8.3 Check for Stability

The maximum buckling stress of a vertical stiffener can be estimated using the following expression [5.76].

$$\sigma_{max} = \frac{N_y}{A} + \frac{M_y \cdot c}{I_{xx}} \sec \frac{\ell}{2} \sqrt{\frac{N_y}{EI_{xx}}}$$

where c is the distance between axes x-x and A-A on Figure 5.53. All other notations being the same as defined in the preceding pages.

$$\sigma_{max} = \frac{600}{23.31} + \frac{16,656 \times 1.33}{80.61} \sec \frac{18 \times 12}{2} \times$$

$$\times \sqrt{\frac{600}{30 \times 10^6 \times 80.61}}$$

$$= 25.74 + 274.81 =$$

$$= 301 \text{ psi.} \quad \text{Hence quite safe}$$

8.4 Design of Horizontal Stiffeners

The most critical value of bending moment appears in elements 118 and 119 i.e. 1826 lbs-in/in of the plate, Tables 5.10 and 5.11.

Similar to the design of vertical girders, using 24 in. as the contributing width of the stack plate,

Total Moment = 1826 × 24 = 43,823 lbs in

Using $\sigma_{all} = 20,000$ psi; the Section modulus required is

$$= \frac{43,824}{20,000} = 2.19 \text{ in}^3$$

The section modulus provided by the composite section in the y-direction is 65.79 in^3. Hence adequately safe.

Therefore, for both vertical stiffeners and horizontal girders around the opening WF 6 shape @ 15.5 should be satisfactory.

REFERENCES — CHAPTER 5

[5.1] Handbook of Industrial Loss Prevent. Prepared by the Staff of the Factory Mutual Engineering Division. General Specifications for the Construction of New Self-Supporting and Guyed Stacks, McGraw-Hill Book Co., N.Y., 1968, pp. 71-7 to 71-11.

[5.2] Ketchum, M.S., Structural Engineers' Handbook, Chapter XI A, Self-Suporting Steel Stacks, McGraw-Hill Book Co., N.Y., 1924, pp. 471-492.

[5.3] British Standards Institution, Specification for Steel Chimney, B.S. 4076: 1966, London, pp. 1-26.

[5.4] British Standard Institution, Code of Basic Data for the Design of Buildings, Chapter V. Loading, Part 1, Dead and Imposed Loads, CP3: 1967, p.6.

[5.5] Steel Stacks. Computation and Construction Design, German Standards DIN 4133, Project, November, 1970, pp. 20. (in German).

[5.6] ACI Committee 307: Proposed Revision of ACI 505-54: Specification for the Design and Construction of Reinforced Concrete Chimneys, ACI Journal. Sept. 1968, pp. 689-712.

[5.7] Abbett, R.W., American Civil Engineering Practice, Vol. III, Reinforced-Concrete Chimneys, John Wiley & Sons, Inc., N.Y., 1957, pp. 32-02 to 32.24.

[5.8] National Research Council of Canada, Canadian Structural Design Manual, Supplement No. 4, to the National Building Code of Canada, 1977, pp. 16, 31, 33.

[5.9] American National Standard Building Code Requirements for Minimum Design Loads in Buildings and Other Structures, 1972, pp. 24, 25.

[5.10] Omori, F., "Wind Pressure on Tall Chimney", Engineering, Vol. 106, 1918.

[5.11] Pagon, W.W., "Vibration Problem in Tall Stacks Solved by Aerodynamics", Eng. News-Record, Vol. 113, No. 2, July 12th, 1934, pp. 41-43.

[5.12] Scruton, C., "Wind-Excited Oscillations of Tall Stacks", The Engineer, June 10th, 1955, pp. 805-808.

[5.13] Ozker, M.S., and Smith, J.O., "Factors Influencing the Dynamic Behavior of Tall Stacks Under the Action of Wind", Trans. of the ASME, Vol. 78, No. 6, August 1956, pp. 1381-1391.

[5.14] Dockstader, E.A., Swiger, W.F., and Ireland, E., "Resonant Vibration of Steel Stacks", Trans. ASCE, Vol. 121, Paper No. 2832, pp. 1088-1112, 1956.

[5.15] Dickey, W.L., and Woodruff, G.B., "The Vibrations of Steel Stacks", Trans. ASCE, Vol. 121, Paper No. 2831, pp. 1054-1087, 1956.

[5.16] Penzien, J., "Wind Induced Vibration of Circular Cylinders", ASCE, Eng. Mech. Div. Proc. Paper 1141, Jan. 1957.

[5.17] Fujino et al, "The Dynamic Behavior of Tall Stacks Under the Action of the Wind", Proc. 7th Nat. Congr. Appl. Mech., Tokyo, 1957, pp. 387-392.

[5.18] Cohen, E., and Perrin, H., "Design of Multilevel Guyed Towers", Papers 1355, 1356, Journ. of St. Div. Proc. ASCE, Vol. 83, St. 5, Sept. 1957.

[5.19] Scruton, C., and Flint, A.R., "Wind-Excited Oscillations of Structures", Proc. Inst. of Civ. Engrs., No. 677, April, 1964.

[5.20] Krupka, V., Design Analysis of Thin-Walled Cylindrical Structures, Praha 1967, Chapter 7 pp. 219-233, (in Czechoslovakian).

[5.21] Nakao, Y., Yamashita, M., Ogata, Y., and Matsumoto, T., "Structural Study on Assembled Four-Cylinder Type Stacks", Technical Review, Mitsubishi Heavy Industries Ltd., January, 1968, pp. 1-10.

[5.22] Vandeghen, A., and Alexandre, M., "Vibrations of the Tall Steel Chimneys Under Wind Action", Publications Internat. Assoc. for Bridge and Struct. Eng., Vol. 29-1, 1969, pp. 95-132, (in French).

[5.23] Wootton, L.R., "The Oscillations of Large Circular Stacks in Wind", Proc. Inst. of Civ. Engrs., Aug. 1969, pp. 573-598.

[5.24] Vellozzi, J., and Cohen, E., "Dynamic Response of Tall Flexible Structures to Wind Loading, Wind Loads on Buildings and Structures", U.S. Dept. of Commerce Publication, Building Science Series 30, 1970, pp. 115-128.

[5.25] Uzsoy, S.Z., "Approximate Analysis of Multiple Circular Cylindrical Shell Wind Shields for High Factory Chimneys", Bull. Int. Assoc. for Shell Structures, No. 41, March, 1970, pp. 43-52, and No. 42, June, 1970, pp. 3-28.

[5.26] Rumman, W.S., "Basic Structural Design of Concrete Chimneys", J. of the Power Div., Proceedings ASCE, June, 1970, pp. 309-318.

[5.27] Anonymous, "Steel Chimney in Trouble", Metal Construction, Vol. 3, No. 4, April, 1971, pp. 145-146.

[5.28] Irish, K., and Cochrane, R.G., "Wind-Induced Oscillation of Circular Chimneys and Stacks", The Structural Engineer, No. 6, Vol. 49, June, 1971, pp. 255-259.

[5.29] Wills, L.G., "Periodic Oscillation of Chimneys", Concrete, May, 1972, p. 35.

[5.30] Irish, K., and Cochrane, R.G., "Wind Vibration of Chimneys", ACI Journal, Sept., 1972, pp. 589-596.

[5.31] Dickey, W.L., "The Design of Two Steam Electric Plants", Trans. ASCE, 1954, Paper No. 2900, pp. 253-272.

[5.32] Dockstader, E.A., Swiga, W.F. and Ireland, E., "Resonant Vibration of Steel Stacks", Proc. ASCE, No. 541, Nov. 1954.

[5.33] Den Hartog, J.P., Mechanical Vibrations, McGraw-Hill Book Co., N.Y., 1947.

[5.34] Dickey, W.L., and Woodruff, G.B., "Vibration of Steel Stacks", Proc. ASCE, No. 540, Nov. 1954.

[5.35] Dockstader, E.A., Swiger, W.F., and Ireland, E., "Resonant Vibration of Steel Stacks", Proc. ASCE, No. 541, November, 1954.

[5.36] Farquharson, F.B., "Wind Forces on Structures: Structures Subject to Oscillation", J. Struct. Div. Proc. ASCE, July, 1958, Paper 1712, pp. 1712-1 and 1712-13.

[5.37] Scrunton, C., "Structures Subject to Oscillation, Discussion of Paper by Farguharson, F.W.", J. Struct. Div., Proc. ASCE, Vol. 85, March, 1959, p. 187.

[5.38] Blume, J.A., "Structural Dynamics in Earthquake Resistant Design", Trans. ASCE, Vol. 125, pp. 1088-1139.

[5.39] Blume, J.A., "A Structural-Dynamic Analysis of Steel Plant Structures Subjected to the May 1960 Chilean Earthquakes", Bulletin of the Seism. Soc. of America, Vol. 53, No. 2, Feb. 1963, pp. 439-48.

[5.40] Kuwano, K., Nakao, Y., Ogato, Y., and Oba, K., "Study on the Seismic Responses of Cylindrical Stacks", Technical Review, Mitsubishi Heavy Industries, Ltd., May 1966, pp. 123-126.

[5.41] Maugh, L.C., and Rumman, W.C., "Dynamic Design of Reinforced Concrete Chimneys", ACI Journal, Proceedings, Vol. 64, No. 9, sept. 1967, pp. 558-567.

[5.42] American Concrete Institute, Specification for the Design and Construction of Reinforced Concrete Chimneys, Standard prepared by ACI Committee 307 (Formerly 503), 1968.

[5.43] Nakao, Y., Yamashita, M., Ogata, Y., and Matsumoto, T., "Structural Study on Assembled Four-Cylinder Type Stacks", Technical Review, Mitsubishi Heavy Industries, Ltd., Jan. 1968, pp. 1-10.

[5.44] Ledwon, J., and Gill, B., "Dynamics of Industrial Chimneys Under Seismic Loads", Intern. Civil Engin, No. 1, Jan. 1969, pp. 10-20.

[5.45] Design Essentials in Earthquake Resistant Buildings, Part 16.3, "Chimneys", Elsevier Publishing Company, N.Y., 1970, pp. 285-287.

[5.46] American National Standard Building Code Requirements for Minimum Design Loads in Buildings and Other Structures, 1972, pp. 25-34.

[5.47] Structural Engineers Association of California, Seismology Committee. Recommended Lateral Force Requirements and Commentary, 1967.

[5.48] Mitchell, W.W., "Determination of the Period of Vibration of Multi-Diameter Columns by the Method Based on Rayleigh's Principle", an unpublished work prepared for the Engineering Department of the Standard Oil Co. of Calif., San Francisco, 1962.

[5.49] Rinne, J.E., "Design of Earthquake-Resistant Structures: Towers and Chimneys", Earthquake Engineering, R.L. Wiegel-Editor, Chapt. 20, Prentice-Hall, Inc. Englewood Cliffs. N.J., 1970, pp. 495-505.

[5.50] Troitsky, M.S., "Design Recommendations Covering Combined Loading Cases and Allowable Stresses for Thin-Walled Cylinders of Large Diameter", CSICC Project #724, 1st Progress Report: Steel Chimneys, Sir George Williams University, January 1973, pp. 1-108.

[5.51] Troitsky, M.S., "Design Recommendations Covering Combined Loading Cases and Allowable Stresses for Thin-Walled Cylinders of Large Diameter", CSICC Project #724, 4th Progress Report: Design Guidelines for Steel Tubular Thin-Walled Structures, Sir George Williams University, January 1974, pp. 1-196.

[5.52] Taylor, F.W., Thompson, S.E., and Smulski, E., Concrete Plain and Reinforced, Vol. 1, John Wiley & Sons, Inc., New York, 4th ed., 1925, pp. 812-819.

[5.53] Timoshenko, S., and Woinowsky-Krieger, S., Theory of Plates and Shells, McGraw-Hill Book Co., Inc., New York, 1959, p. 210.

[5.54] Brownell, L.E., and Young, E.H., Process Equipment Design-Vessel Design, John Wiley & Sons, Inc., New York, 1968, pp. 183-197.

[5.55] Troitsky, M.S., "Design Recommendations Covering Combined Loading Cases and Allowable Stresses for Thin-Walled Cylinders of Large Diameter", CSICC Project #724, 5th Progress Report: Breech Openings at Steel Stacks, Guidelines for Analysis and Design, Concordia University, January 1978, pp. 1-131.

[5.56] Brogan, F. and Almroth, B.O., "Buckling of Cylinders With Cutouts", AIAA Journal, Vol. 8, No. 2, Feb. 1970, pp. 236-241.

[5.57] Almroth, B.O. and Homes, A.M.C., "Buckling of Shells With Cutouts, Experiment and Analysis", Int. J. Solids Structures, Vol. 8, 1972, pp. 1057-1071.

[5.58] Structural Stability Research Council, Guide to Stability Design Criteria for Metal Structures, 3rd ed., Ed. by B.G. Johnston, John Wiley & Sons, New York, U.S.A., 1976, p. 193.

[5.59] Inglis, C.E., "Stresses in a Plate due to the Presence of Cracks and Sharp Corners", Trans. Inst. Nav. Arch., Vol. 55, 1913, pp. 219-230.

[5.60] Savin, G.N., Stress Concentration Around Holes, Pergamon Press, New York, 1961.

[5.61] Greenspan, M., "Effect of a Small Hole on the Stresses in a Uniformly Loaded Plate", Quart. Appl. Mech., Vol. 2, No. 1, 1944, pp. 60-71.

[5.62] Brock, J.S., "Analytical Determination of the Stresses Around Square Holes With Rounded Corners", DTMB Report 1149, Nov. 1957.

[5.63] Muskhelishvili, N.I., Some Basic Problems of the Mathematical Theory of Elasticity, (translation by J.R.M. Radok), P. Noordhoff Ltd., Groningen, Holland, 1953.

[5.64] Brogan, F.A. and Almroth, B.O., "Buckling of Cylinders With Cutouts", AIAA Jnl. 8, pp. 236-241, (1970).

[5.65] Almroth, B.O., Brogan, F.A. and Marlowe, M.B., "Collapse Analysis for Elliptic Cones", AIAA Jnl. 9, pp. 32-36, (1971).

[5.66] Almroth, B.O. and Brogan, F.A., "Collapse Analysis for Shells of General Shape", Vol. I AFFDL-TR-71-8, Wright-Patterson Air Force Base, Ohio, (1971).

[5.67] Holmes, A.M.C. and Almroth, B.O., "An Experimental Study of the Strength and Stability of Thin Monocoque Shells With Reinforced and Unreinforced Rectangular Cutouts". Final Report Under Contract NAS9-10372, prepared for NASA/Manned Spacecraft Centre, Houston, Texas.

[5.68] Almroth, B.O., Brogan, F.A. and Zele, F., "Collapse Analysis for Shells of General Shape", Vol. II, User's Manual for STAGS, AFFDL-TR-71-8, Wright-Patterson Air Force Base, Ohio, (1971).

[5.69] Turner, M.J., Clough, R.W., Martin, H.C. and Topp, L.J., "Stiffness and Deflection Analysis of Complex Structures", J. Aero, S., Vol. 23, No. 9, 1956, pp. 805-823.

[5.70] Argyris, J.H. and Kelsey, S., Energy Theorems and Structural Analysis, Butterworths, London, 1960 (Collection of papers published in Aircraft Engineering in 1954 and 1955).

[5.71] Bathe, K.J., Wilson, E.L. and Peterson, F.E., SAP IV; "A Structural Analysis Program for Static and Dynamic Response of Linear Systems", Report EERC-73-11, Earthquake Engineering Research Centre, University of California, Berkeley, June 1973 (PB-221-967/3, N.T.I.S.).

[5.72] Zienkiewicz, O.C., The Finite Element Method in Engineering Science, McGraw-Hill Company, London, 1971.

[5.73] Wilson, E.L., Taylor, R.L., Doherty, W.P. and Ghaboussi, J., Incompatible Displacement Models, Numerical and Computer Methods in Structural Mechanics, edited by S.J. Fenves, et al., Academic Press, Inc. N.Y. and London, 1973.

[5.74] DeSalvo, G.J. and Swanson, J.A., ANSYS – Engineering Analysis System: User's Manual, Swanson Analysis Systems, Inc., 879 Pine View Drive, Elizabeth, Pennsylvania, 15037.

[5.75] American Institute of Steel Construction, Manual of Steel Construction, 6th ed., 1967, New York.

[5.76] Johnston, B.G., Guide to Stability Design Criteria for Metal Structures, 3rd ed., John Wiley & Sons, New York, 1967, pp. 26-77.